

AD-A070 954

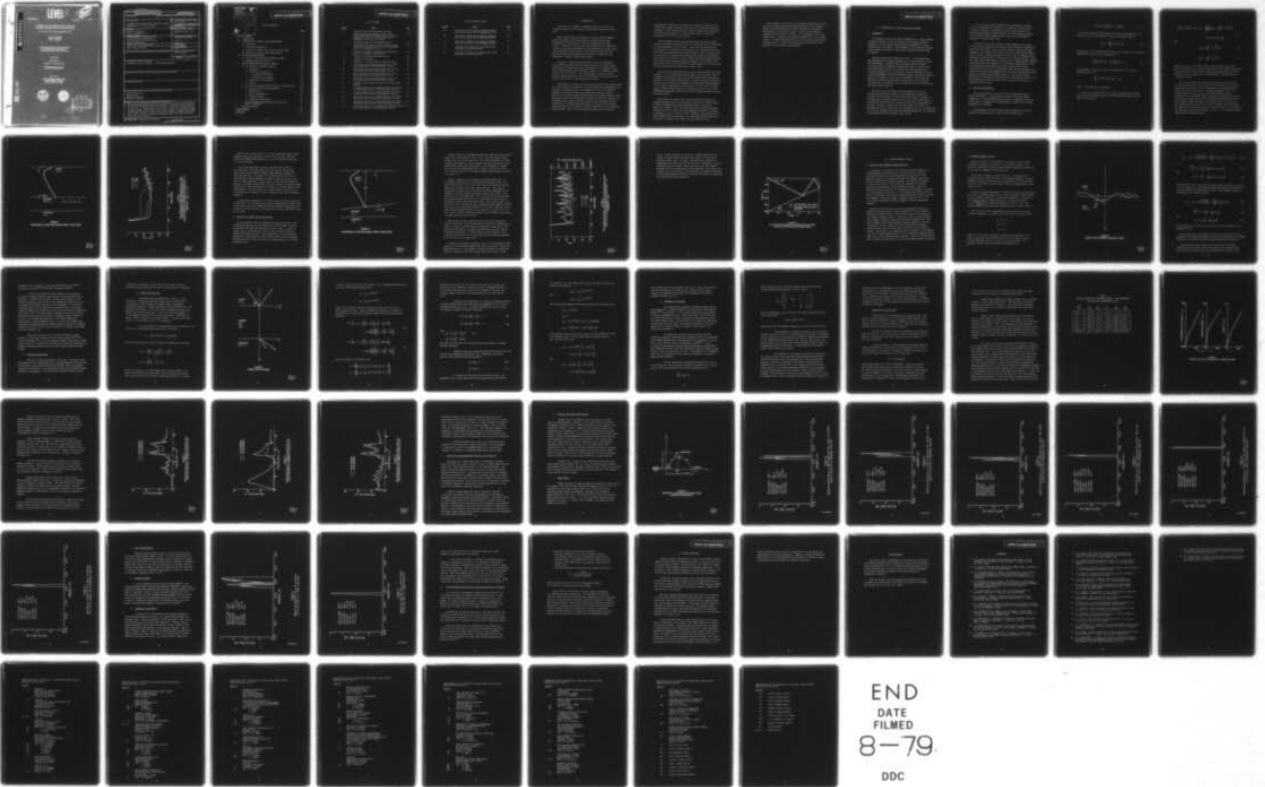
TEXAS UNIV AT AUSTIN APPLIED RESEARCH LABS
A SUMMARY OF THE RESULTS OF A STUDY OF ACOUSTIC INTERACTION WIT--ETC(U)
MAR 79 K E HAWKER, S R RUTHERFORD, P J VIDMAR N00014-78-C-0113
ARL-TR-79-2

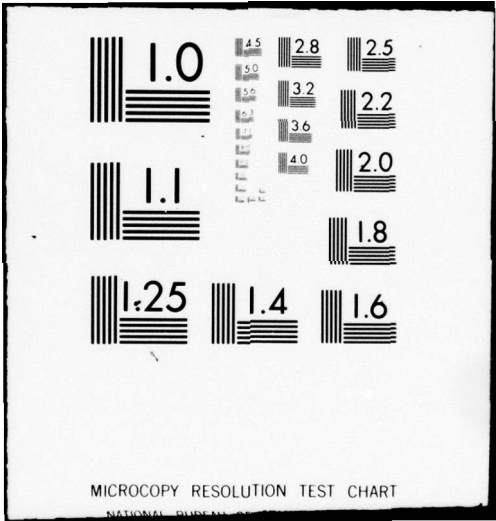
F/G 20/1

UNCLASSIFIED

NL

| OF |
AD
A070954





ADA070954

LEVEL

J 

copy no. 62

ARL-TR-79-2

A SUMMARY OF THE RESULTS OF A STUDY OF ACOUSTIC INTERACTION WITH THE SEA FLOOR

Annual Report under Contract N00014-78-C-0113

Kenneth E. Hawker
Steven R. Rutherford
Paul J. Vidmar

APPLIED RESEARCH LABORATORIES
THE UNIVERSITY OF TEXAS AT AUSTIN
POST OFFICE BOX 8029, AUSTIN, TEXAS 78712

5 March 1979

Annual Report

1 January - 31 December 1978

APPROVED FOR PUBLIC RELEASE;
DISTRIBUTION UNLIMITED

Prepared for:

NAVAL OCEAN RESEARCH AND
DEVELOPMENT ACTIVITY
NSTL STATION, MS 39529

DDC FILE COPY



DDC
RECEIVED
JUL 6 1979
REGULATED
P

79 07 25 068

UNCLASSIFIED

SECURITY CLASSIFICATION OF THIS PAGE (When Data Entered)

REPORT DOCUMENTATION PAGE		READ INSTRUCTIONS BEFORE COMPLETING FORM
1. REPORT NUMBER	2. GOVT ACCESSION NO.	3. RECIPIENT'S CATALOG NUMBER
4. TITLE (and Subtitle)		5. TYPE OF REPORT & PERIOD COVERED
6. A SUMMARY OF THE RESULTS OF A STUDY OF ACOUSTIC INTERACTION WITH THE SEA FLOOR		Annual Report 1 January-31 December 1978
7. AUTHOR(s)		8. PERFORMING ORG. REPORT NUMBER
Kenneth E. Hawker Steven R. Rutherford Paul J. Vidmar		14 ARL-TR-79-2
9. PERFORMING ORGANIZATION NAME AND ADDRESS		9. CONTRACT OR GRANT NUMBER(s)
Applied Research Laboratories The University of Texas at Austin Austin, Texas 78712		15 N00014-78-C-0113
11. CONTROLLING OFFICE NAME AND ADDRESS		10. PROGRAM ELEMENT, PROJECT, TASK AREA & WORK UNIT NUMBERS
Naval Ocean Research and Development Activity NSTL Station MS 39529		12 82P.1
14. MONITORING AGENCY NAME & ADDRESS (if different from Controlling Office)		12. REPORT DATE
		11 5 March 1979
		13. NUMBER OF PAGES
		78
		15. SECURITY CLASS. (of this report)
		UNCLASSIFIED
		15a. DECLASSIFICATION/DOWNGRADING SCHEDULE
		N/A
16. DISTRIBUTION STATEMENT (of this Report)		
APPROVED FOR PUBLIC RELEASE; DISTRIBUTION UNLIMITED.		
17. DISTRIBUTION STATEMENT (of the abstract entered in Block 20, if different from Report)		
18. SUPPLEMENTARY NOTES		
19. KEY WORDS (Continue on reverse side if necessary and identify by block number)		
Bottom interaction Geoacoustics Doppler broadening Mode-mode coupling		
20. ABSTRACT (Continue on reverse side if necessary and identify by block number)		
(U) This report summarizes the results of research carried out during 1978 at Applied Research Laboratories, The University of Texas at Austin (ARL:UT) on acoustics interaction with the sea floor. Major topics considered are propagation in a range variable environment by mode-mode coupling methods, bottom roughness (scattering) studies, and a number of sensitivity studies including the acoustical effects of sediment rigidity, Doppler broadening due to source motion, and the relationship between mode attenuation and bottom loss per bounce. ←		

DD FORM 1 JAN 73 1473

EDITION OF 1 NOV 65 IS OBSOLETE

UNCLASSIFIED

SECURITY CLASSIFICATION OF THIS PAGE (When Data Entered)

404 434

JCB

NTIS GRA&I		<input checked="" type="checkbox"/>
DDC TAB		
Unannounced		<input type="checkbox"/>
Justification		<input type="checkbox"/>
By _____		
Distribution/ _____		
Availability Codes _____		
Distrib.	Avail and/or special	
A		

PRECEDING PAGE BLANK-NOT FILMED

TABLE OF CONTENTS

	<u>Page</u>
LIST OF FIGURES	v
I. INTRODUCTION	1
II. PROPAGATION IN A RANGE VARIABLE ENVIRONMENT	5
A. Motivation	5
B. Theoretical Background	6
C. Results for Lateral Variations in the Sea Floor	9
D. Results for Sloping Bottom Applications	13
III. BOTTOM ROUGHNESS STUDIES	19
A. Review of Water-Sediment Roughness Studies	19
B. Basement Roughness Studies	20
IV. BOTTOM INTERACTION SENSITIVITY STUDIES	25
A. The Effects of Sediment Rigidity	25
1. Background	25
2. Theoretical Background	26
a. Differential Equations	27
b. Mathematical Formalism	32
3. Computation of Bottom Loss	34
4. Results	39
B. Bottom Interacting Multipath Effects on Line Structure	44
1. Receiver and Source Depth Effects	45
2. Range Effects	45
3. Source Speed Effects	55
4. Frequency Effects	55
5. Integration Time Effects	55
C. The Relationship Between Mode Attenuation and Bottom Loss/Bounce	58
V. SUPPORT ACTIVITIES	61
ACKNOWLEDGMENTS	63
REFERENCES	65

LIST OF FIGURES

<u>Figure</u>	<u>Title</u>	<u>Page</u>
1	Waveguide Layer and Sound Speed Structure	11
2	Relationship Between Sediment Radial Sound Speed Gradient and Mode Number such that Milder's Adiabatic Criterion is satisfied for $\epsilon=0.1$, Frequency = 20 Hz, and $g = 1 \text{ sec}^{-1}$	12
3	Waveguide Layer and Sound Speed Structure	14
4	Relationship Between Local Bottom Slope and Mode Number such that Milder's Criterion is Satisfied for $\epsilon=0.1$, Frequency = 20 Hz	16
5	Ray Trace Performed by Conventional Methods and Within the Context of Mode Theory	18
6	Geometry for Basement Roughness Theory	21
7	Schematic of the Model	28
8	Parameters of the Hypothetical Turbidite Layer	37
9	Reflection Loss versus Grazing Angle for a 518 m Thick Hypothetical Turbidite Layer at 20 Hz	38
10	Reflection Loss versus Grazing Angle for a 252 m Thick Hypothetical Turbidite Layer at 20 Hz	41
11	Reflection Loss versus Grazing Angle for a 36 m Thick Hypothetical Turbidite Layer at 20 Hz	42
12	Reflection Loss versus Grazing Angle for a 36 m Thick Hypothetical Turbidite Layer at 200 Hz	43
13	Schematic Illustration of Source Track and Receiver Geometry	46
14	Normalized Spectrum at a 1000 m Receiver for a 25 Hz, 5 m Deep Source Located 20 km Downrange from CPA	47
15	Normalized Spectrum at a 4500 m Receiver for a 25 Hz, 5 m Deep Source Located 20 km Downrange from CPA	48
16	Normalized Spectrum at a 1000 m Receiver for a 25 Hz, 100 m Deep Source Located 20 km Downrange from CPA	49
17	Normalized Spectrum at a 4500 m Receiver for a 25 Hz, 100 m Deep Source Located 20 km Downrange from CPA	50
18	Normalized Spectrum at a Receiver 50 m Above the Bottom for a 25 Hz Source, 200 km Downrange from CPA	51

LIST OF FIGURES (Cont'd)

<u>Figure</u>	<u>Title</u>	<u>Page</u>
19	Spectrum at a Receiver 50 m Above the Bottom for a 25 Hz Source, 100 km Downrange from CPA	52
20	Spectrum at a Receiver 50 m Above the Bottom for a 25 Hz Source, 50 km Downrange from CPA	53
21	Spectrum at a Receiver 50 m Above the Bottom for a 25 Hz Source, 10 km Downrange from CPA	54
22	Normalized Spectrum for a 15 kt Source 20 km from CPA, at a 1000 m Receiver	56
23	Normalized Spectrum for a 100 Hz Source 20 km from CPA, at a 4500 m Receiver	57

I. INTRODUCTION

This report is a summary of research carried out as part of a continuing study of the interaction of underwater sound with the sea floor.

Under a wide variety of conditions of source-receiver geometry, acoustic frequency, sound speed profile, and water depth, sound propagation in the ocean can be heavily influenced by the ocean bottom. Although sea floor structure and composition has itself been a subject for study by geophysicists and seismologists for many years, only comparatively recently has it been appreciated that sea floor makeup can impact sound propagation over ranges, frequencies, and geometries of concern to Naval applications.

The scope of these applications which must be concerned with bottom effects includes system performance prediction, system design, interpretation of acoustical data, the integration of geophysical data into acoustic modeling, and the design of experiments intended to gather acoustic data in the ocean. This broad range of concerns in which acoustic bottom interaction can play a significant role requires various levels of description of bottom interaction effects.

Traditionally, the nature of bottom interaction has been characterized by a single quantity, bottom loss. For many applications knowledge of this quantity is indeed sufficient, for example, in ray trace estimates of propagation loss used in some system performance prediction models. However, more complex problems involving phase interference between various multipaths, such as the functioning of arrays, the nature of Doppler line broadening, and a range of problems concerned with multipath, or mode conversion due to range changing bathymetry, all require more detailed characterization of the sea floor if these phenomena are to be understood quantitatively. Many of these problems may require fairly detailed

descriptions of subbottom sound speed and attenuation profiles as well as location of major interfaces (reflectors) and possibly of shear wave parameters. Such problems go beyond a simple regional characterization of bottom loss estimated in 1/3 octave bands, however useful such information may be for certain problems.

Applied Research Laboratories, The University of Texas at Austin (ARL:UT), has been conducting a study of the influence of the ocean bottom on sound propagation characteristics. In view of the various levels of description of the ocean bottom required by the intended applications, this study has encompassed three primary research areas: (1) sensitivity of bottom loss to variations and uncertainties in subbottom parameters, (2) the role of the bottom in various range changing environment problems, particularly slope coupling and bottom roughness, and (3) bottom interaction effects such as those involved in array studies, cw line structure, and the interpretation of experimental acoustic data.

From the outset the primary goals of this research program have been fourfold: (1) to determine and provide guidance on the level of detail of subbottom parameters required for acoustic applications (sensitivity studies), (2) to determine which aspects of mode, or multipath conversion caused by slope coupling, and roughness, are predictable and exploitable, (3) to develop computational tools appropriate to the study of a wide range of complex bottom interaction problems, and (4) to interact with experimental measurement programs via exercise planning and data analysis and interpretation.

During FY78, as reported here, research is being carried out on problems associated with slope coupling, the effects of lateral changes in subbottom composition, bottom roughness effects, and various sensitivity studies. Much of the work during FY78 has been to develop computational tools to deal with these problems, and much of this work is expected to come to fruition in FY79. Examples of such work would be slope coupling problems approached via a mode-mode coupling study, and the effects of sediment shear waves on bottom reflection loss.

The remainder of this report is divided into three major sections dealing with range changing environment problems, bottom roughness studies, and bottom interaction sensitivity studies. Substantial documentation, in the form of papers or reports, gives detailed expositions of the bulk of this work. As a consequence, this report attempts only to summarize the technical approach and to give example results. It should be appreciated that every important research area discussed here is a subject of continuing work with results to be expected in the directions indicated here.

II. PROPAGATION IN A RANGE VARIABLE ENVIRONMENT

A. Motivation

The purpose of this year's work on propagation in a range dependent environment has been to lay the foundation for studying a number of problems of current interest involving sound propagation in a range variable ocean environment. These problems can be divided into sloping bottom studies and studies of the effects of lateral subbottom range variability.

Specific problems to be addressed include: (1) determining the depth dependence of average propagation loss in the presence of slopes, with applications to ambient noise and signal-to-noise problems, (2) partitioning of propagated energy between water and bottom paths, (3) arrival angle structure for receivers and arrays located near continental slopes, and (4) the influence of slope subbottom structure on slope enhancement, bottom interference effects, and array performance. Theoretical parameter studies and the development of analytical and numerical computational techniques will emphasize use of a detailed description of the subbottom. These studies will use data from previous and ongoing ARL:UT projects.

The work carried out during FY78, and summarized here, has successfully produced the analytical and computational methods and computer software necessary to attack this broad range of problems. It is recognized, and indeed essential, that at this early stage certain problems may be addressed with a level of detail that is unnecessary for practical solutions. Since one of the objectives of this work is to determine the level of detail that will be required, not only in describing the sea floor acoustically but also in modeling propagation, the investigation should proceed from a general point of view.

In the studies of lateral subbottom range variability, emphasis will be on determining the sensitivity of propagation characteristics to lateral variations in subbottom structure. Such variations can arise from nonhorizontal layering beneath the water-sediment interface, or from gradual lateral changes within a layer due to differential deposition of varying grain sizes.

In order to attack the problem of sound propagation in a region of bottom range variability, one needs to select the proper computational approach to the problem. Since the main concern is with bottom range variability, the coupled mode theory of Pierce¹ and Milder² was selected since it allows a complete description of the bottom. Software has been developed for computation of acoustic fields in a range dependent environment using coupled mode theory, in particular, for computing mode coupling coefficients and radial equations in the adiabatic approximation. Also, work has been done using analytical radial solutions and coupling coefficients in an effort to understand the mode coupling process and to understand the physical phenomena without the massive computational effort required in a general mode coupling solution. Sensitivity studies dealing with the influence of bottom type on the adiabatic solution to the radial equation were also carried out this year and the results are summarized in this report.

B. Theoretical Background

The starting point for this work is the coupled mode theory of Pierce¹ and Milder.² In this theory one seeks to describe acoustic propagation in a range dependent medium within a formalism in which the normal modes of propagation in the waveguide are coupled via the range dependence of the medium.

The development of the coupled mode theory begins with the three-dimensional wave equation for a point source located at \vec{x}_0 .

$$\nabla^2 \psi(\vec{x}) + k^2(\vec{x})\psi(\vec{x}) = -4\pi\delta(\vec{x}-\vec{x}_0) \quad (1)$$

For a medium having azimuthal symmetry and radial range dependence, the solution to Eq. (1) is expressed in partially separated form as

$$\psi(r,z) = \sum_n R_n(r) \phi_n(z,r) \quad , \quad (2)$$

where $\psi(r,z)$ is the velocity potential and $\phi_n(z,r)$ satisfies the following differential equation at each range point r :

$$\left[\frac{\partial^2}{\partial z^2} + k^2(r,z) - k_n^2(r) \right] \phi_n(z,r) = 0 \quad (3)$$

At each range r , the $\phi_n(z,r)$ form an orthonormal set of functions normalized such that

$$\int_0^\infty \rho \phi_n(z,r) \phi_m^*(z,r) dz = \delta_{n,m} \quad , \quad (4)$$

where ρ is the density of the medium.

If Eq. (2) is inserted in Eq. (1) and the orthonormality property of Eq. (4) is exploited, one may obtain the following equation for the radial function $R_m(r)$.

$$\frac{d^2}{dr^2} R_m + \frac{1}{r} \frac{d}{dr} R_m + k_m^2(r) R_m = - \sum_n \left\{ A_{mn} R_n + B_{mn} \left(\frac{R_n}{r} + 2 \frac{d}{dr} R_n \right) - \frac{2}{r} \delta(r) \rho(z_0) \phi_m(z_0, r) \right\} \quad (5)$$

with

$$A_{mn}(r) = \int_0^\infty \rho \phi_m \frac{\partial^2 \phi_n}{\partial r^2} dz \quad (6)$$

$$B_{mn}(r) = \int_0^\infty \rho \phi_m \frac{\partial \phi_n}{\partial r} dz \quad (7)$$

Equation (5) is a set of coupled radial equations and the $A_{mn}(r)$ and $B_{mn}(r)$ are referred to as coupling coefficients. The coupling coefficients are proportional to radial rates of change of mode amplitudes, and their presence in Eq. (5) gives rise to a redistribution of modal energies as a function of range.

Since the numerical and computational techniques for calculating the mode functions of Eq. (3) are well in hand, the main effort involved in the coupled mode approach is to calculate the coupling coefficients of Eqs. (6) and (7) and to solve the range equation (Eq. (5)). The coupling coefficients A_{mn} and B_{mn} are perhaps the most important functions in the coupled mode theory since both the numerical procedures for solving the range equation and the simplifying approximations to the range equation depend critically on the range behavior of the B_{mn} and A_{mn} . Therefore it is necessary to be able to compute these coefficients as quickly and efficiently as possible. Computer code is now in existence for computing the coupling coefficients of Eq. (7) for a completely general range variable propagation geometry.

If the terms involving mode coupling in Eq. (5) are, in some sense, small compared to the other terms of the equation, it makes sense to employ the adiabatic approximation to Eq. (5). Within this approximation, Eq. (5) becomes

$$\frac{d^2}{dr^2} R_m + \frac{1}{r} \frac{d}{dr} R_m + k_m^2(r) R_m = - \frac{2\delta(r)}{r} \rho(z_0) \phi_m(z_0, r) \quad (8)$$

Since the radial equations in the adiabatic approximation are many times easier to solve than the coupled radial equations, it is extremely useful to be able to estimate the magnitude of sediment range variations that may be tolerated within the adiabatic approximation. Computer code has been written to solve Eq. (8) in a general range changing environment. An analytic solution to Eq. (8) for an isovelocity, wedge shaped ocean has also been developed and some results obtained through its use will be presented.

C. Results for Lateral Variations in the Sea Floor

The first work done using the numerical tools developed this year deals with the validity and sensitivity of the adiabatic approximation as a function of the range dependence of sediment geoaoustic parameters (see Refs. 3 and 4). This work contains elements of both the sloping bottom and lateral inhomogeneity problems.

There are several criteria for the validity of the adiabatic approximation; the one selected for use in this work was derived by Milder and involves a comparison of the coupling coefficients B_{mn} with the eigenvalue spacing. Using this criterion, the adiabatic approximation is valid if

$$\left| \frac{B_{m,m+1} X_m}{\pi} \right| = \epsilon \ll 1 \quad , \quad (9)$$

where X_m is the mode cycle distance given by

$$X_m = \frac{2\pi}{k_m - k_{m+1}} .$$

Hence, if the mode coupling over a mode cycle is small, then adiabatic mode invariance is expected.

The first range dependent parameter investigated was the sediment sound speed. Figure 1 depicts the waveguide geometry used in the numerical calculations that were performed. The first layer is a water layer 4500 m deep having an arbitrary sound speed profile (for the calculations presented in this paper a mid-Pacific type profile was used). The sediment layer is 300 m deep and is dependent on range and depth as

$$c_2(r,z) = c_0(r) + g(z-H) .$$

This investigation of the radial sediment sound speed gradient falls into the lateral subbottom inhomogeneity category.

Figure 2 depicts the relationship between mode number and local radial sound speed derivative such that Eq. (9) is satisfied for $\epsilon=0.1$. The frequency was taken to be 20 Hz and the sediment was modeled as either clay, silt, or sand. There are about 106 discrete modes for this frequency and layering geometry. Several interesting features are evident in this figure. First, note the large dip in the curves at about mode No. 24. This dip marks the dividing line between modes with turning points in the water and those with turning points in the sediment. For modes with $m < 24$ one sees very little influence from the range variation of the sediment sound speed.

The main findings of this portion of this work may be summarized as follows.

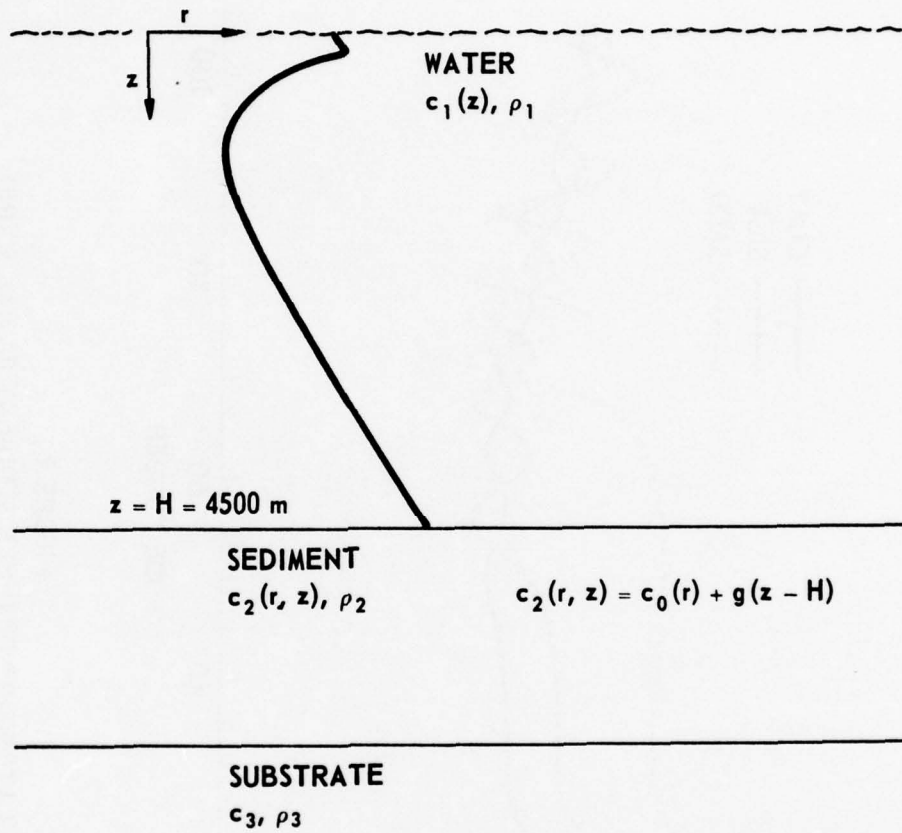


FIGURE 1
WAVEGUIDE LAYER AND SOUND SPEED STRUCTURE

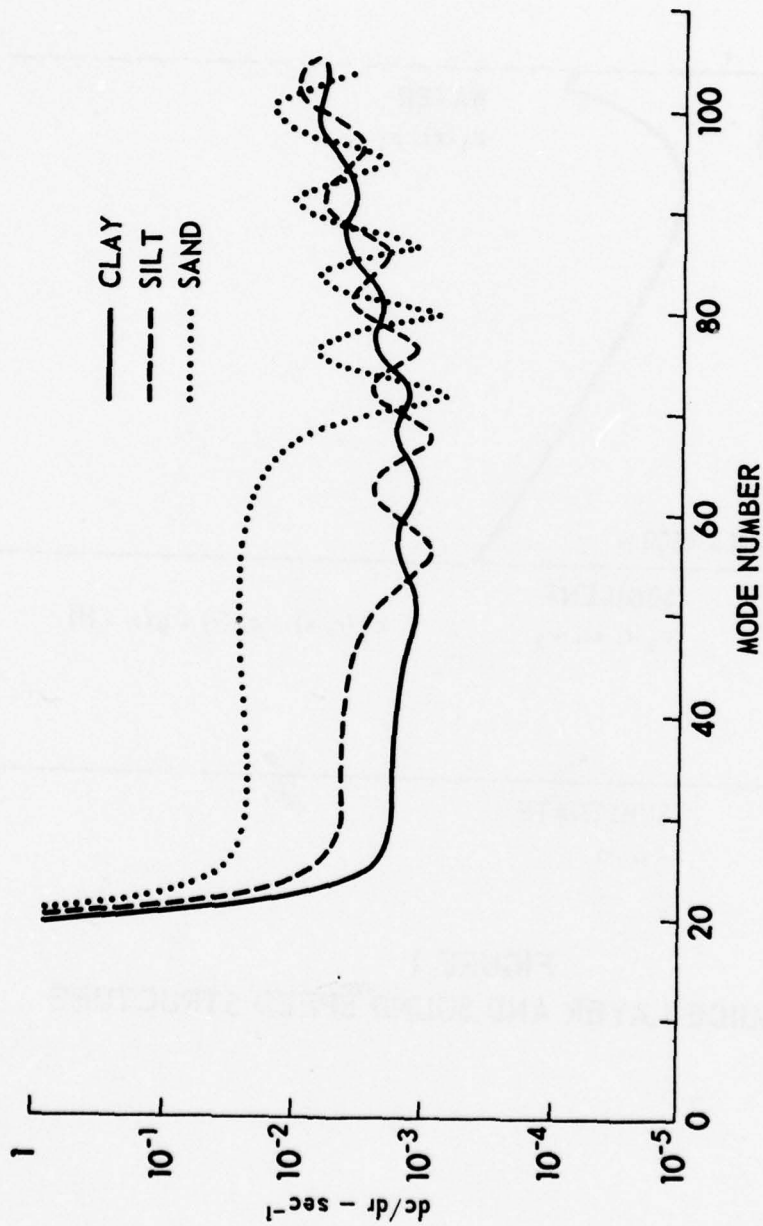


FIGURE 2
 RELATIONSHIP BETWEEN SEDIMENT RADIAL SOUND
 SPEED GRADIENT AND MODE NUMBER SUCH THAT
 MILDNER'S ADIABATIC CRITERION IS SATISFIED FOR $\epsilon = 0.1$,
 FREQUENCY = 20 Hz, $g = 1 \text{ sec}^{-1}$

Based on Fig. 2 and a choice of $\epsilon=0.1$ it can be said that a radial sediment sound speed gradient of about 10^{-3} sec^{-1} may be tolerated within the adiabatic approximation for all of the sediment types and for all mode numbers.

In the lower mode number portion (less than $m \approx 60$) of Fig. 2 the curves are in the order sand, silt, and clay; in this low mode region sand can withstand the highest radial gradients followed by silt, and then clay. This behavior is related to the fact that the characteristic acoustic impedance of sand is higher than that of silt, which is higher than that of clay. Hence, for the low mode numbers in question, the sand bottom contains the lowest fraction of acoustic energy present and is least affected by the presence of a radial sediment sound speed gradient. Silt is affected to a greater degree than sand since its characteristic impedance is less, followed by clay with the smallest impedance.

In long range propagation, it is likely that only the lower modes are of importance. In a situation such as this the magnitude of radial sound speed gradient that may be handled within the adiabatic approximation can be seen to vary over an order of magnitude as the bottom type varies from clay to sand.

D. Results for Sloping Bottom Applications

The next parameter that was examined was local bottom slope. The waveguide geometry used for calculation of the normal modes, coupling coefficients, and mode cycle distances is shown in Fig. 3. There is a water layer of variable depth given by $H(r)$ overlying isovelocity sediment and substrate layers. The calculations to be presented were performed at a range where the water depth was 4500 m and the sediment thickness was 300 m. Again, the water sound speed profile is a typical mid-Pacific type.

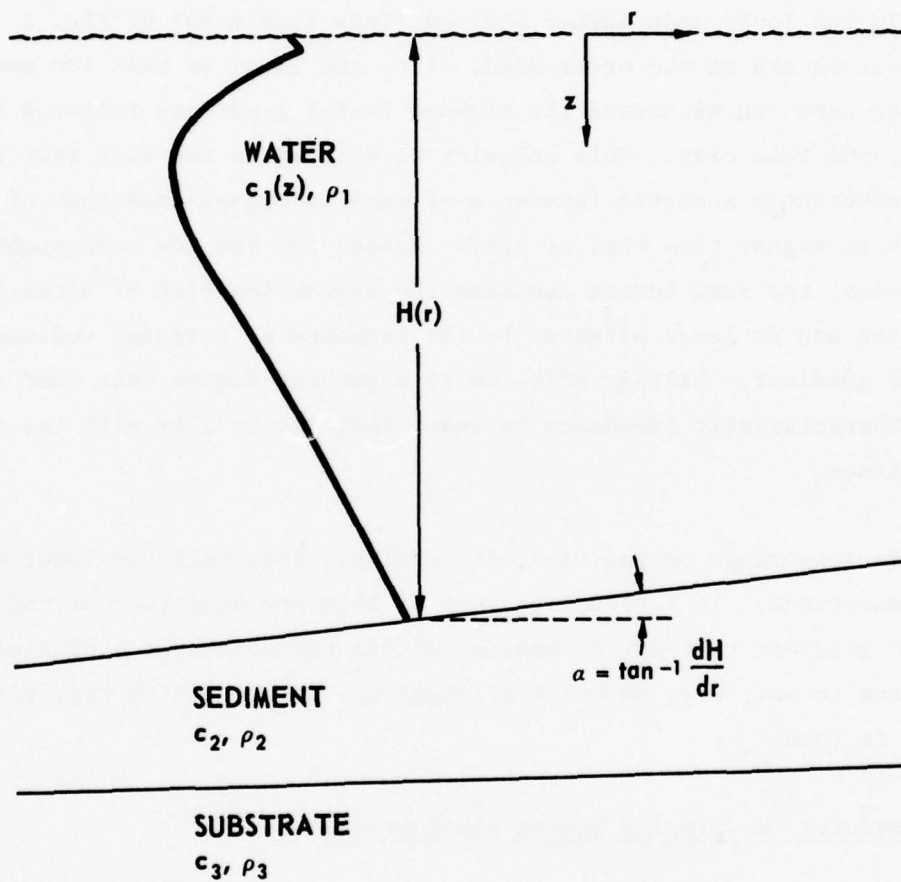


FIGURE 3
 WAVEGUIDE LAYER AND SOUND SPEED STRUCTURE

Figure 4 shows the relationship between mode number and local bottom slope, dH/dr , satisfying Eq. (9) for $\epsilon=0.1$, with the sediment being treated as a clay, a silt, and sand. For a given mode number m , values of dH/dr lying beneath a curve correspond to slopes that may be treated adiabatically, while those lying above a curve correspond to slopes that may not be treated adiabatically. Based on the choice of $\epsilon=0.1$, Fig. 4 reveals that most of the modes propagate adiabatically for slopes up to about 0.5° .

Figure 4 summarizes our findings concerning the sensitivity of the adiabatic approximation to bottom slope and sediment type. Note that the curves tend to lie in the order clay, silt, and sand with clay being able to tolerate more slope angle than sand. This ordering follows the ordering of the characteristic acoustic impedances of the sediments, with clay having the smallest and sand the largest. This behavior is not inconsistent with one's intuition that an acoustically hard, sloping bottom would give rise to more mode conversion than an acoustically softer, more penetrable bottom. The curves in Fig. 4, for the choice $\epsilon=0.1$, indicate that mode conversion effects begin to arise in sand for local bottom slopes between 0.057° and 0.57° , whereas for clay, mode conversion effects begin at slope angles on the order of 0.5° to 1.0° . Hence, the mode conversion process due to a sloping bottom seems to be fairly sensitive to bottom type.

Another piece of work completed this contract year concerns the relation between ray theory and mode theory concepts in a sloping bottom region. The basic question examined concerns the relationship of the coupling coefficients to the physically meaningful ray theory concept of multipath conversion. In other words, is it the presence of the coupling coefficients in Eq. (5) that gives rise to multipath phenomena or do they play a more subtle role?

To address this problem, an analytic solution to the adiabatic range equation for an isovelocity wedge shaped ocean was derived. Using this analytic solution, it was possible to extend the methods of Tindle and Guthrie⁵ to perform a ray trace entirely within the context of mode

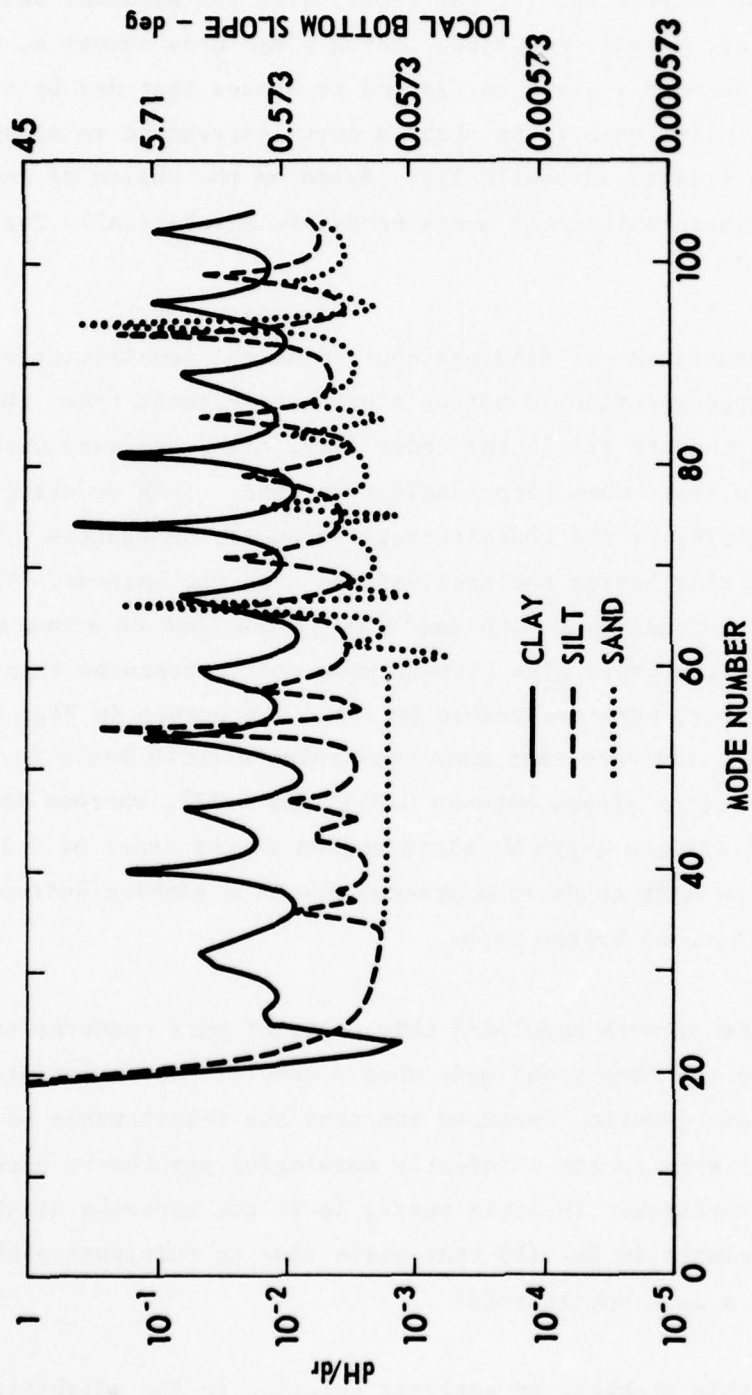


FIGURE 4
 RELATIONSHIP BETWEEN LOCAL BOTTOM SLOPE AND MODE NUMBER
 SUCH THAT MILDER'S CRITERION IS SATISFIED FOR $\epsilon = 0.1$,
 FREQUENCY = 20 Hz

theory. Figure 5 depicts a ray trace for a source located at the surface at a point where the water depth is 500 m. The bottom was treated as rigid, with a 10° slope. The solid curve represents a conventional ray theory ray trace and the circles represent a ray trace performed using the adiabatic radial solution. Note the excellent agreement even for the large (10°) slope considered. This leads one to conclude that the adiabatic solution describes the geometric properties of the sound propagation while the coupling coefficients are responsible for redistributing modal amplitudes.

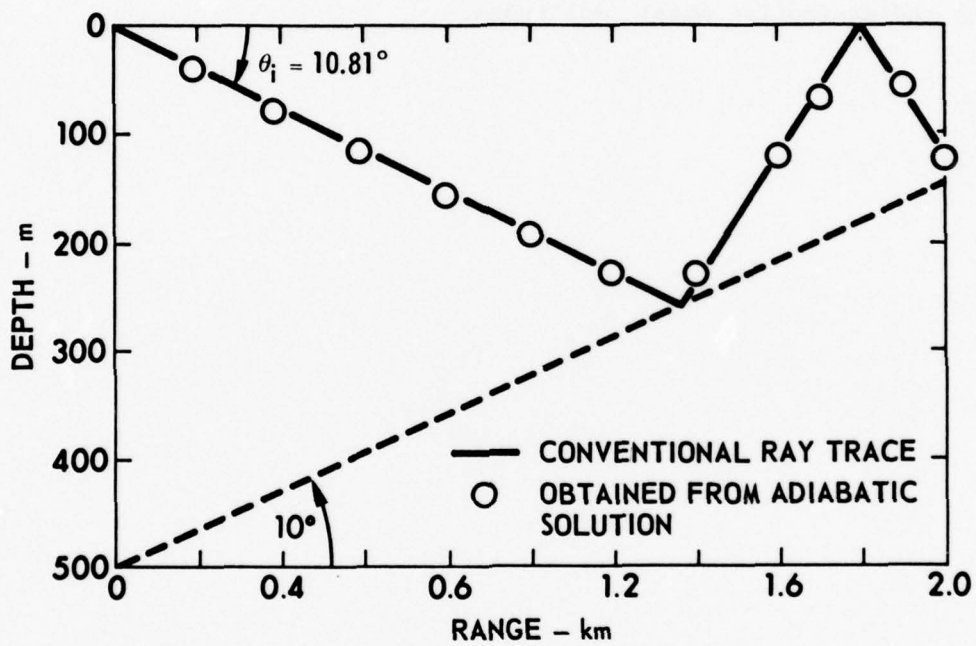


FIGURE 5
 RAY TRACE PERFORMED BY CONVENTIONAL METHODS
 AND WITHIN THE CONTEXT OF MODE THEORY

ARL:UT
 AS-78-1647-P
 SRR - GA
 10 - 26 - 78

III. BOTTOM ROUGHNESS STUDIES

A. Review of Water-Sediment Roughness Studies

The problem of accounting for the effects of bottom roughness on sound propagation characteristics is a very difficult one that has received the attention of many researchers over a period of years. Since the inception of this bottom interaction program a small effort has been devoted to this specific problem. In particular, the goals of this work have been to first assess the usefulness of existing methods for accounting for bottom roughness and then to carry out sensitivity studies using the most promising of these methods. The goals of the sensitivity studies are: (1) to determine the required level of detail of description of subbottom roughness (How much do we have to know, rms roughness, correlation length, correlation function, etc.), and (2) to assess the impact of bottom roughness effects on surveillance problems.

Beginning in FY77, efforts in this area were based entirely on a smoothed or average boundary condition approach;^{6,7} such an approach was found by previous study to offer the best method for accounting for low frequency roughness effects. Sensitivity study results concerning water-sediment interface roughness were published during FY78.⁸ These results suggested that water-sediment interface roughness is probably not important, at low frequencies, and for high porosity sediments (clays and silts) such as those found in deep ocean basins (abyssal plains). During FY78 it was suggested that, for regions of thin sediment cover such as the Northeast Pacific, the most important roughness effects might occur at the sediment-basement interface. Work was initiated during FY78 to extend existing theory to include the sediment-basement interface.

B. Basement Roughness Studies

During FY78 the work of Kuperman⁶ on the randomly rough two-fluid interface was extended to the case of a fluid-solid interface. The aim was to calculate the specular reflection and transmission coefficients of the coherent component of the sound field.

The geometry considered is shown in Fig. 6. A two-dimensional coordinate system is used with the z axis increasing downward. The fluid (medium 1) and the solid (medium 2) are separated by the interface given by $z=\alpha(x)$. The origin, $z=0$, is chosen so that the average height of the surface is zero.

The exact boundary conditions at a point on the surface $(x_0, \alpha(x_0))$ are written in a coordinate system (x', z') in Fig. (6) whose z axis is normal to the interface at that point. The boundary condition is converted to the original coordinate system by means of a rotation by an angle $\theta = \tan^{-1} \left(\frac{d\alpha}{dx} \Big|_{x_0} \right)$ and a translation along the z axis of $\alpha(x_0)$. The resulting boundary conditions are expanded about $z=0$ to second order in α .

The next step involves the separation of the fields into mean and stochastic components. In terms of scalar and vector potentials this is

$$\phi_1 = \phi_1 + v_1 \quad ,$$

$$\phi_2 = \phi_2 + v_2 \quad ,$$

$$\psi = \Psi + w \quad ,$$

where ϕ_1, ϕ_2 are scalar potentials; ψ is the vector potential in the solid; v_1, v_2 , and w are stochastic fields (in the variable x) due to the rough interface; and ϕ_1, ϕ_2 , and Ψ are the mean fields. The boundary conditions can now be ensemble averaged to give

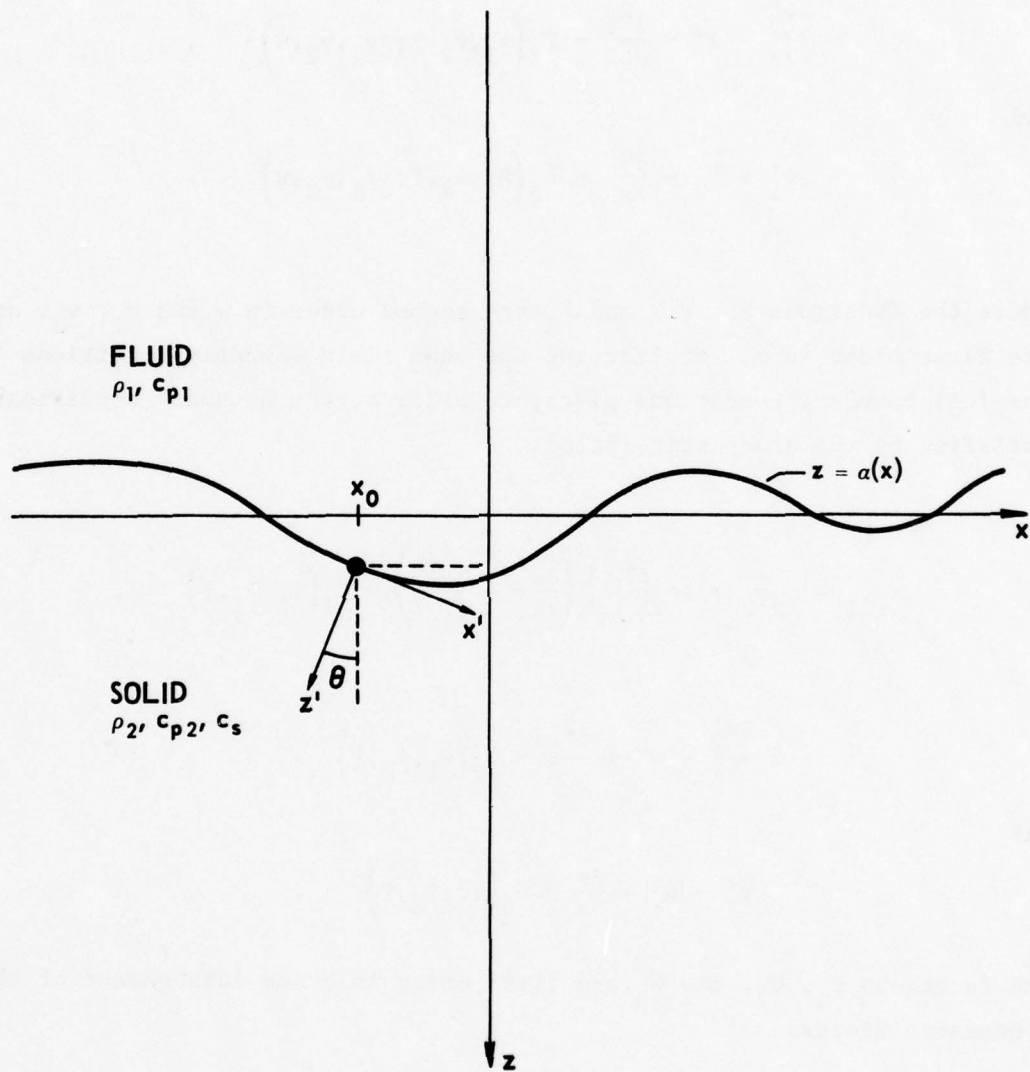


FIGURE 6
 GEOMETRY FOR BASEMENT ROUGHNESS THEORY

ARL:UT
 AS-78-2014
 PJV-GA
 1-3-79

$$\rho_1 \phi_1' - \rho_2 \phi_2' + 2\rho_2 \left(\frac{c_s}{\omega}\right)^2 \left(\frac{\partial \psi'}{\partial x} - \frac{\partial^2 \phi}{\partial x^2}\right) = F_1(\phi_1, \phi_2, \psi; v_1, v_2, w) \quad , \quad (10)$$

$$2 \frac{\partial \phi_2'}{\partial x} - \psi'' + \frac{\partial^2 \phi}{\partial x^2} = F_2(\phi_1, \phi_2, \psi; v_1, v_2, w) \quad , \quad (11)$$

and

$$\phi_1' - \phi_2' - \frac{\partial \psi}{\partial x} = F_3(\phi_1, \phi_2, \psi; v_1, v_2, w) \quad , \quad (12)$$

where the functions F_1 , F_2 , and F_3 are second order in α and v_1 , v_2 , and w are first order in α . Subtracting the mean field boundary conditions from the full boundary conditions gives, to order α , the boundary conditions satisfied by the stochastic fields:

$$\rho_1 v_1' - \rho_2 v_2' + 2\rho_2 \left(\frac{c_s}{\omega}\right)^2 \left(\frac{\partial w'}{\partial x} - \frac{\partial^2 v_2}{\partial x^2}\right) = G_1(\phi_1, \phi_2, \psi) \quad , \quad (13)$$

$$2 \frac{\partial v_2'}{\partial x} - w'' + \frac{\partial^2 w}{\partial x^2} = G_2(\phi_1, \phi_2, \psi) \quad , \quad (14)$$

and

$$v_1' - v_2' - \frac{\partial w}{\partial x} = G_3(\phi_1, \phi_2, \psi) \quad . \quad (15)$$

The functions G_1 , G_2 , and G_3 are first order in α and independent of the stochastic fields.

At this point Eqs. (10) through (12) state that the correction due to roughness in the specular direction is of order α^2 because Eqs. (10) through (12) reduce to the plane interface boundary conditions if $F_1 = F_2 = F_3 = 0$.

The procedure for calculating the reflection and transmission coefficients is as follows. First set $F_1 = F_2 = F_3 = 0$ and, assuming plane waves, solve for the zero order (in α) fields at the interface. These

can then be used to calculate G_1 , G_2 , and G_3 . Equations (13) through (15) are then used to obtain the stochastic fields in terms of the zero order fields. The zero order fields and the stochastic fields are then used to calculate F_1 , F_2 , and F_3 . Equations (10) through (12), after subtracting the zero order fields, are then used to calculate the second order correction to the mean fields. Assuming a unity amplitude incoming wave will yield the correction to the reflection and transmission coefficients.

The theory outlined above is complete and in a form suitable for numerical computation. Work is in progress to develop computer software for carrying out these computations. The results of sensitivity studies to be carried out using these methods will be reported during the next fiscal year.

IV. BOTTOM INTERACTION SENSITIVITY STUDIES

A continuing aspect of the bottom interaction studies at ARL:UT has been the use of various "measures" of bottom interaction as vehicles to test the importance of one or more parameter variations or uncertainties. In the beginning a commonly used measure was propagation loss, and work was carried out to determine the sensitivity of propagation loss to variations in bottom loss. More recent studies have explored the acoustical importance of various sea floor parameters such as density, sound speed, and absorption gradient using bottom reflection loss as a measure of bottom interaction.

Sections following deal with two additional elements in this line of investigation: one, the effect of sediment rigidity, again uses bottom reflection loss as the measure; the other concerns the effects of bottom interaction on cw line spectra. A third section is concerned with the relationship between two commonly used measures, bottom reflection loss per bounce and mode attenuation.

A. The Effects of Sediment Rigidity1. Background

In FY76 a study was begun of the sensitivity of bottom reflection loss to subbottom parameter variations. Initially the work concentrated on the properties of a fluid sediment and was carried out using a sophisticated bottom reflection loss model⁹ developed at ARL:UT for this purpose. This model treats the sediment as a fluid. The unique feature of the model is its use of direct numerical integration to solve the wave equation. This permits arbitrary depth variations to be treated accurately and without resort to approximation. As a research tool the model has proved to be very flexible and convenient to use. Various sea floor

parameters such as density,¹⁰ sound speed and absorption gradients,¹¹ and substrate rigidity^{12,13} have been successfully studied.

In FY78 the direction of these studies turned toward the inclusion of sediment rigidity (shear waves) in the bottom reflection loss model. Guided by the success of the ARL:UT fluid model, it was decided to develop a model based on direct numerical integration for use in studying the acoustic properties of solid sediments. The necessary theoretical work has been completed and translated into an operating computer program which computes the bottom reflection loss for frequencies above about 10 Hz. This model makes it possible, for the first time, to quantitatively estimate the importance of sediment rigidity within the context of an inhomogeneous geoacoustic model without making the approximation of many homogeneous layers. A second, more complex (and computer time consuming) model is being developed to extend the frequency range down to about 3 Hz and verify the accuracy of the basic solid model at its low frequency end.

Useful and realistic results have been obtained by using estimates of shear wave parameters from the work of Hamilton^{14,15} and Shirley and Hampton,¹⁶ to constrain parameter ranges in sensitivity studies. Initial studies of a hypothetical turbidite layer have been completed and suggest that sediment shear waves may be more important than heretofore thought.

2. Theoretical Background

Theoretical work was necessary in two areas. The first was the determination of the appropriate form of the depth separated wave equations to be solved. Major considerations were the direct effect of parameter gradients and the effect of coupling between shear and compressional waves induced by the gradients. The second area of theoretical work involved

developing a formalism for calculating the plane wave reflection coefficient which would allow the use of direct numerical integration.

a. Differential Equations

The model is shown schematically in Fig. 7. A two-dimensional, horizontally stratified ocean bottom is considered. It is composed of a solid sediment overlying a solid, homogeneous, semiinfinite substrate. Sediment parameter values are permitted to vary arbitrarily with depth. Solid lines indicate compressional waves and dashed lines indicate shear waves. The z axis increases downward. H is the sediment thickness and θ is the grazing angle. Subscripts are used to identify quantities in different media: 0 refers to the water column, 1 to the sediment, and 2 to the substrate.

At low frequencies the displacement \underline{u} in the sediment can be written in a generalized potential form due to Richards¹⁷

$$\underline{u}_1 = \frac{1}{f_1(z)} \nabla P_1(x, z, t) + \frac{1}{F_1(z)} \nabla \times Q_1$$

The scale functions $f_1(z)$ and $F_1(z)$ satisfy the differential equations

$$G_1(z) \equiv \frac{F_1'(z)}{F_1(z)} = \frac{v_1^2}{c_1^2 - v_1^2} \left(\frac{\rho_1'}{\rho_1} + 4 \frac{v_1'}{v_1} \right)$$

$$g_1(z) \equiv \frac{f_1'(z)}{f_1(z)} = \frac{\rho_1'}{\rho_1} - G_1(z) \quad ,$$

where ρ_1 is density, c_1 is sound speed, and v_1 is shear speed, all of which are permitted to vary arbitrarily, but continuously, with depth. The scale functions have the initial conditions $F_1(0)=f(0)=1$. A prime

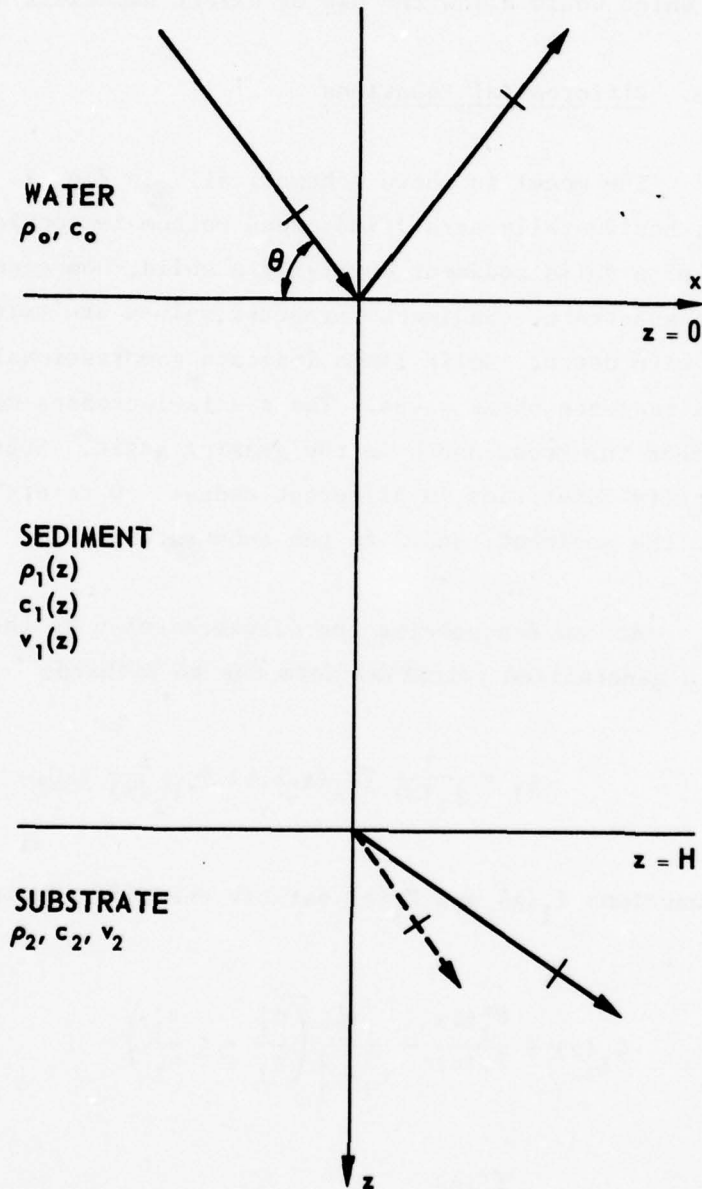


FIGURE 7
SCHEMATIC OF THE MODEL

ARL:UT
AS-78-1733-S
PJV - GA
11-27-78

is used to denote a derivative with respect to z . Decomposing the potentials P_1 and Q_1 , assuming plane waves, gives

$$P_1 = \phi_1(z) e^{i(kx - \omega t)}$$

$$Q_1 = \hat{y}\psi_1(z) e^{i(kx - \omega t)},$$

where ω is the angular frequency, $k = k_o \sin\theta$, $k_o = \omega/c_o$, and \hat{y} is a unit vector along the y axis. Using the equations of motion, the approach of Richards¹⁹ can be applied and extended to obtain the closed form coupled equations:

$$\begin{aligned} \phi_1'' + \left(G_1 - g_1 - \frac{D_1'}{D_1} \right) \phi_1' + \frac{D_1}{d_1} \left(d_1 \frac{\omega^2}{c_1^2} - k_o^2 \cos^2 \theta \right) \phi_1 \\ = i k_o \cos \theta \left(\frac{f_1}{F_1} \right) \left[\frac{D_1'}{D_1} \psi_1 + \left(\frac{D_1}{d_1} - 1 \right) \psi_1' \right], \end{aligned} \quad (16)$$

$$\begin{aligned} \psi_1'' + \left(g_1 - G_1 - \frac{d_1'}{d_1} \right) \psi_1' + \frac{d_1}{D_1} \left(D_1 \frac{\omega^2}{v_1^2} - k_o^2 \cos^2 \theta \right) \psi_1 \\ = -i k_o \cos \theta \left(\frac{F_1}{f_1} \right) \left[\frac{d_1'}{d_1} \phi_1 + \left(\frac{d_1}{D_1} - 1 \right) \phi_1' \right], \end{aligned} \quad (17)$$

where $d_1 = 1 - (b_1/\omega^2)$, $D_1 = 1 - (B_1/\omega^2)$, and

$$\begin{aligned} b_1 &= v_1^2 \left[\left(\rho_1' g_1 / \rho_1 \right) + \left(2 v_1' g_1 / v_1 \right) + g_1' - g_1^2 \right], \\ B_1 &= c_1^2 \left[\left(\rho_1' G_1 / \rho_1 \right) + \left(2 c_1' G_1 / c_1 \right) + G_1' - G_1^2 \right]. \end{aligned}$$

Equations (16) and (17) are equivalent to the equations of motion and are valid at all frequencies. The direct effect of gradients appears in the ϕ_1' and ψ_1' terms on the left side of the equations. The right side of these equations describes coupling between shear and compressional waves.

Estimates of the magnitude of b_1 and B_1 for gradients typical of marine sediments show that this coupling is negligible ($d \approx 1$, $D \approx 1$) for frequencies above about 3 Hz. For higher frequencies we can set $d_1 = D_1 = 1$ and $d_1' = D_1' = 0$ to obtain the uncoupled equations

$$\phi_1'' + (G_1 - g_1)\phi_1' + K_1^2\phi_1 = 0 \quad , \quad (18)$$

$$\psi_1'' + (g_1 - G_1)\psi_1' + \beta_1^2\psi_1 = 0 \quad , \quad (19)$$

where

$$K_1^2 = \left(\omega/c_1\right)^2 - k_o^2 \cos^2 \theta \quad , \text{ and}$$

$$\beta_1^2 = \left(\omega/v_1\right)^2 - k_o^2 \cos^2 \theta \quad .$$

Equations (18) and (19) still contain the terms due directly to physical parameter gradients.

Estimates of g_1 and G_1 show that the second terms in Eqs. (18) and (19) can be neglected above about 10 Hz. Neglecting these terms results in the simplified description given by

$$\phi_1'' + K_1^2\phi_1 = 0 \quad , \quad (20)$$

$$\psi_1'' + \beta_1^2\psi_1 = 0 \quad . \quad (21)$$

To complete the description of the acoustic field, the components of the stress tensor which are continuous across an interface

are required, i.e., the normal stresses p_{jzz} , and shear stresses p_{jzx} . These can be written as

$$p_{jzz} = \sigma_{jzz}(z) e^{i(kx - \omega t)},$$

and

$$p_{jzx} = \sigma_{jzx}(z) e^{i(kx - \omega t)}.$$

For the water and substrate the depth functions have the familiar form

$$\sigma_{ozz} = -\rho_0 \omega^2 \phi_0(z)$$

$$\sigma_{ozx} = 0$$

$$\sigma_{2zz} = -\rho_2 (\omega^2 - 2v_2^2 k^2) \phi_2(z) + 2i\rho_2 v_2^2 k \psi_2'(z)$$

$$\sigma_{2zx} = 2i\rho_2 v_2^2 k \phi_2'(z) + \rho_2 (\omega^2 - 2v_2^2 k^2) \psi_2(z).$$

The presence of scale factors in \underline{u}_1 results in a more complicated result in the sediment layer. For the high frequency uncoupled limit of Eqs. (18) and (19) we have

$$\begin{aligned} \sigma_{1zz} = & -\rho_1 (\omega^2 - 2v_1^2 k^2) \frac{\phi_1}{f_1} - \rho_1 G_1 c_1^2 \frac{\phi_1'}{f_1} \\ & - i\rho_1 G_1 c_1^2 k \frac{\psi_1}{F_1} + 2i\rho_1 v_1^2 k \frac{\psi_1'}{F_1} \end{aligned}$$

and

$$\begin{aligned} \sigma_{1zx} = & -i\rho_1 g_1 v_1^2 k \frac{\phi_1}{f_1} + 2i\rho_1 v_1^2 k \frac{\phi_1'}{f_1} \\ & + \rho_1 (\omega^2 - 2v_1^2 k^2) \frac{\psi_1}{F_1} + \rho_1 g_1 v_1^2 \frac{\psi_1'}{F_1}. \end{aligned}$$

These differ from the usual results in two ways. First, the potentials and their derivatives are scaled by their respective scale factors. Second, new terms appear which depend on the gradients of sediment parameters through g_1 and G_1 .

b. Mathematical Formalism

Most models which include both sediment rigidity and the depth dependence of sediment parameters have been based on the Thomson-Haskell^{18,19} matrix method. In this method gradients are approximated by many thin homogeneous layers. Within each layer the wave equations are solved analytically in terms of upgoing and downgoing plane waves. The matrix approach allows the elimination of most plane wave amplitudes as quantities to be calculated, and compactly represents a structured ocean bottom in terms of only four variables, one of which is the reflection coefficient R.

Our approach is motivated by the success of direct numerical integration in modeling fluid sediments, and by the compactness of the Thomson-Haskell matrix representation of layered solids. Both of these can be combined using the "propagator" formalism.²⁰ In this formalism the differential equations describing shear and compressional wave propagation within a layer are replaced by a matrix relating boundary values at the top and bottom of the layer. The elements of the propagator matrix can be calculated by direct numerical integration of the depth separated wave equations.

The two second-order differential equations for ϕ_1 and ψ_1 can be written as four first-order differential equations for ϕ_1 , ϕ_1' , ψ_1 , and ψ_1' . These four equations can be written in matrix form as

$$\frac{d\phi_1}{dz} = \underline{A}_1(z) \phi_1 \quad ,$$

where $\phi_1 = (\phi_1, \phi_1', \psi_1, \psi_1')$ is the four-component potential vector and the matrix $\underline{A}_1(z)$ representing Eqs. (18) and (19) is

$$\underline{A}_1 = \begin{pmatrix} 0 & 1 & 0 & 0 \\ -K_1^2 & g_1 - G_1 & 0 & 0 \\ 0 & 0 & 0 & 1 \\ 0 & 0 & -B_1^2 & G_1 - g_1 \end{pmatrix}$$

Since the elements of \underline{A}_1 are continuous functions of depth the solution can be written as²⁰

$$\phi_1(H) = \underline{E}_1(H,0) \phi_1(0) ,$$

where $\underline{E}_1(H,0)$ is the propagator relating ϕ_1 at $z=H$ to its value at $z=0$.

The propagator is evaluated by choosing a set of different potential vectors at the top of the sediment and integrating to the bottom. A set of equations in the unknown matrix elements is generated and solved. For the differential equation sets of Eqs. (18) and (19) and Eqs. (20) and (21) there are only eight nonzero matrix elements since the shear and compressional fields are decoupled. In these cases only two properly chosen initial vectors are required.

The procedure for calculating the reflection coefficient is the same as that of the traditional Thomson-Haskell matrix method with the exception of using the propagator to solve the differential equations. Briefly the procedure is as follows. Starting with the potential vector in the water due to the incoming and reflected plane waves, convert to the stress displacement vector and use the continuity of normal displacement and stress and shear stress to cross into the sediment. Converting back to potentials, the propagator is used to cross the sediment layer. Next, the sediment-substrate interface is crossed by

converting to stress displacement, using the continuity conditions and converting back to the potentials due to the shear and compressional plane waves in the substrate. This procedure results in four equations in four unknowns, one of which is the reflection coefficient. Solving the system of equations leads to the reflection coefficient. All possible configurations of fluid or solid sediment and substrate have been treated in the matrix formalism.

3. Computation of Bottom Loss

A model based on the inhomogeneous wave equations (Eqs. (20) and (21)) has been developed into a functioning computer program. This model is the most efficient in terms of computation time, and provides accurate results for frequencies above 10 Hz. The numerical integration technique has been discussed in detail elsewhere.⁹

Efforts are currently under way to implement a model based on Eqs. (18) and (19). This will be used to check the accuracy of the basic model at low frequencies, and also to extend the model capability to yet lower frequencies.

In the basic model at a given frequency and grazing angle the reflection coefficient is calculated for the appropriate case of fluid or solid sediment or substrate. The quantity delivered as output is not R itself but rather the reflection loss (bottom loss),

$$RL = -20 \log_{10}(|R|) \quad ,$$

and the phase angle of R, $\delta = \tan^{-1}[\text{Im}(R)/\text{Re}(R)]$. These are available both as hard copy printout and as a disk file prepared for plotting. Two types of output are possible: (1) RL as a function of grazing angle at a given frequency, or (2) RL as a function of frequency at a given grazing angle. In this latter case the attenuation is assumed to be proportional to frequency^{21,22} and is input normalized to the value at

1 kHz. Because of a local error tolerance feature, execution times increase with wave frequency as wavelengths become small.

Typical input parameters are shown in Table I for the sediment structure of Fig. 8 taken from Fryer.²³ The depth grid on which the parameters are specified is arbitrary. Linear gradients are assumed between grid points. No assumptions are made about the relationship between parameters.

Figure 9 shows typical results obtained for the profile of Fig. 8. Three cases at a frequency of 20 Hz are shown. For a fluid substrate no difference was seen between a solid (dashed curve) and fluid (dotted curve) sediment. For a fluid sediment and solid substrate the expected increase in RL is seen between $\theta_s = 50^\circ$ and $\theta_p = 70^\circ$, where θ_s and θ_p are the critical angles for shear waves and compressional waves in the substrate. For a solid sediment and a solid substrate (solid curve) the resonance structure between θ_s and θ_p is modified. No other major effect is seen.

The correct operation of the program was verified as follows. For a fluid sediment the results for solid and fluid substrate conditions were compared with those obtained from an existing model,⁹ which treats fluid sediments only. For a solid sediment the results for fluid and solid substrates were compared with those obtained for particular choices of depth dependence for which analytic solutions of the wave equations are possible. The reflection coefficient was calculated by solving the set of six (fluid substrate) or seven (solid substrate) simultaneous equations generated by the continuity conditions for a homogeneous sediment. The comparisons showed excellent agreement and thus verified the logic flow of the program and the accuracy of the numerical integrator. In the course of operation one area of inaccuracy has been noted. For small grazing angles and deep sediments, a loss of precision is possible because of the exponential nature of the wave functions. However, this is not a serious

TABLE I
 PHYSICAL PARAMETERS OF SEDIMENT STUDIED. THE ATTENUATIONS
 ARE GIVEN FOR A FREQUENCY OF 20 Hz.

Depth m	c_o m/sec	v_o m/sec	ρ g/cm ³	α_p dB/m	α_s dB/m
Water	1530	---	1.03	---	---
0	1510	116	1.53	0.0013	0.169
36	1582	283	1.579	0.0020	0.112
120	1674	391	1.689	0.0040	0.172
518	1992	621	2.010	0.0027	0.087
Substrate	4460	2400	2.46	0.00016	0.00079

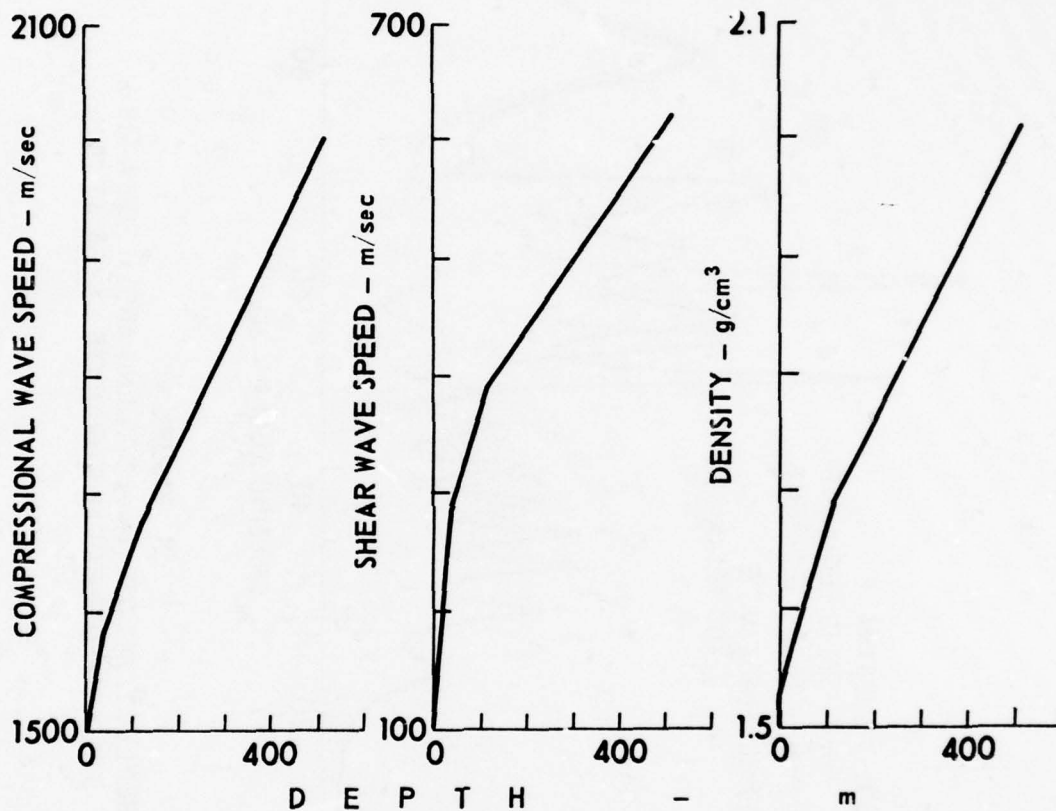


FIGURE 8
PARAMETERS OF THE HYPOTHETICAL TURBIDITE LAYER

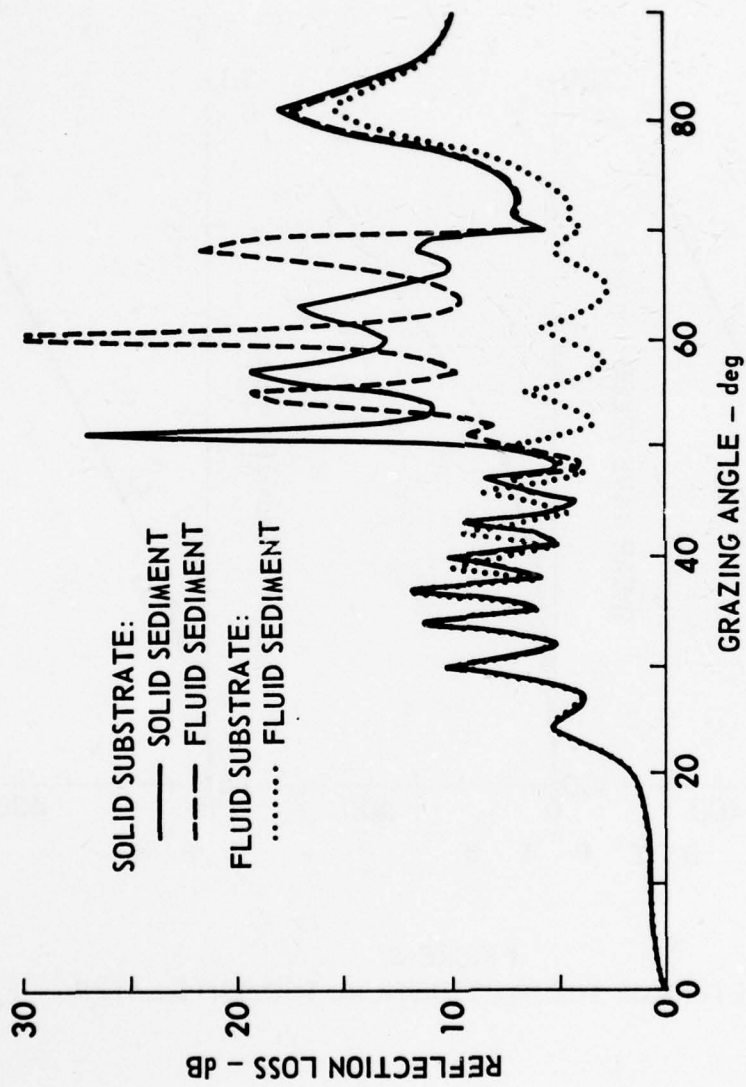


FIGURE 9
 REFLECTION LOSS versus GRAZING ANGLE FOR A 518 m
 THICK HYPOTHETICAL TURBIDITE LAYER AT 20 Hz

ARL:UT
 AS-78-1735-S
 PJV-GA
 11-27-78

problem, since the wave does not penetrate deeply into the sediment and the thickness of the layer can be reduced until accurate results are obtained.

4. Results

This model has been used by Vidmar and Foreman²⁴ to study the effect of sediment rigidity on R for the hypothetical turbidite layer of Fig. 8 which was obtained from Fryer.²³ These parameters represent realistic depth variations as deduced from geophysical data. There are also depth dependent attenuations not shown.

Figure 9 shows a comparison of the calculated reflection coefficients of this sediment for three different bottom configurations at a frequency of 20 Hz. The dotted curve is obtained by setting the shear parameters to zero and corresponds to the case of a fluid sediment and a fluid substrate. The oscillations are due to the interference between the wave reflected directly from the water-sediment interface and the wave penetrating the sediment and returning to the water. To isolate the effect of substrate rigidity, the dashed curve was generated for the case of a fluid sediment but a solid substrate. Comparison with the dotted curve shows that substrate rigidity is responsible for the increased loss and the structure between 50° and 70°. The critical angle for shear wave propagation in the substrate is 50°, and 70° is the critical angle for compressional waves. The increased reflection loss between the two critical angles is due to energy carried away by the substrate shear waves. The effect of sediment rigidity can now be seen by comparing the solid and dashed curves. The solid curve was generated for a solid sediment and substrate. The difference between these two curves is entirely due to sediment rigidity. There is a negligible effect except between the two critical angles; here sediment rigidity produces a shift in the location of the peaks.

Figure 10 shows the effect of sediment rigidity when the sediment thickness is reduced to 252 m, still at 20 Hz. Both curves were obtained for a solid substrate. As in the previous and following figures, the solid curve is for solid sediment and the dashed curve for fluid sediment. In addition to the expected peak shifts between the critical angles, sediment rigidity has the additional effect of increasing the reflection loss above 24° .

As the sediment thickness is further reduced a pattern develops. There is a minimum angle, θ_0 , above which sediment rigidity increases the reflection loss. The angle θ_0 steadily decreases as the thickness decreases. The situation at 36 m thickness is shown in Fig. 11, still at 20 Hz. Here θ_0 has decreased to zero. Sediment rigidity clearly dominates the reflection loss at low angles with a dramatic increase of 20 dB near 13° .

The effect of sediment rigidity is expected to decrease at higher frequencies. Figure 12 shows the reflection loss at 200 Hz for the same 36 m layer. The increased reflection loss is indeed smaller, but is not yet negligible. Even at this relatively high frequency there is an increase of about 4 dB between 15° and 30° .

Several observations can be made based on these results. First, sediment rigidity does matter. Second, the reflection loss depends on layer thickness in a regular fashion. The angle above which sediment rigidity is important increases as the thickness increases. Thirdly, excitation of shear waves at the water-sediment interface is not important, whereas conversion of compressional waves at the substrate interface is dominant.

This last point requires some elaboration. Significant changes in the reflection loss occurred when only the sediment thickness was changed. Since the upper interface parameters were constant, physical processes occurring there are not likely to be the major cause of the

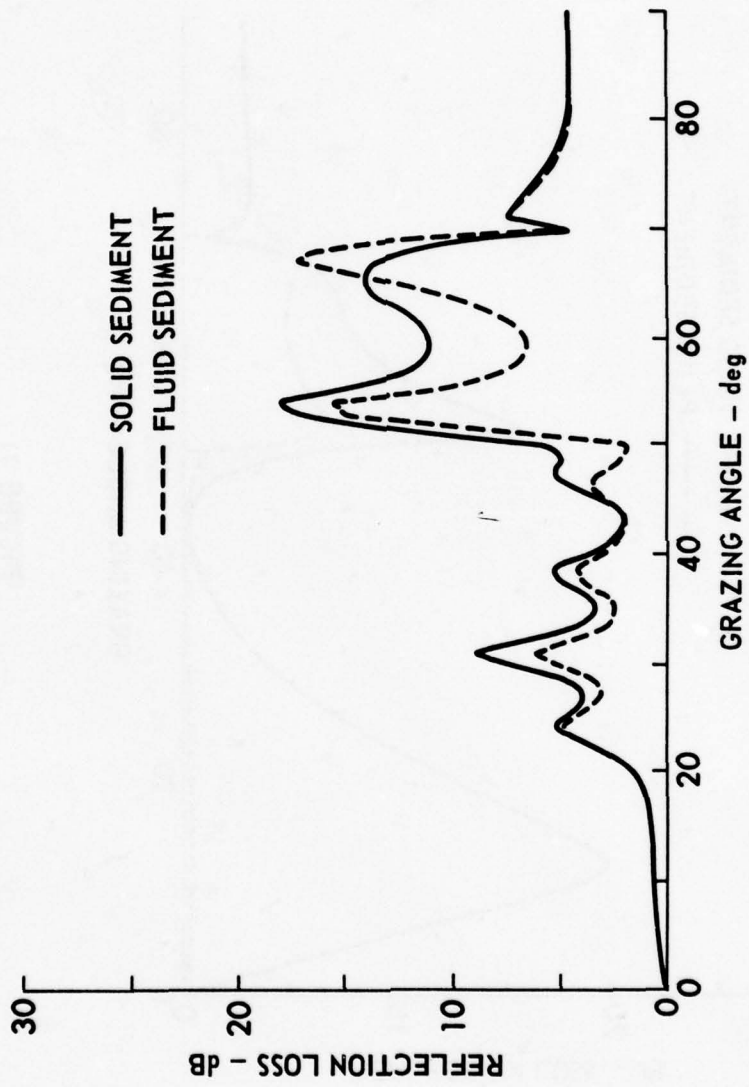


FIGURE 10
 REFLECTION LOSS versus GRAZING ANGLE FOR A 252 m
 THICK HYPOTHETICAL TURBIDITE LAYER AT 20 Hz

ARL:UT
 AS-78-1737-S
 PJV-GA
 11-27-78

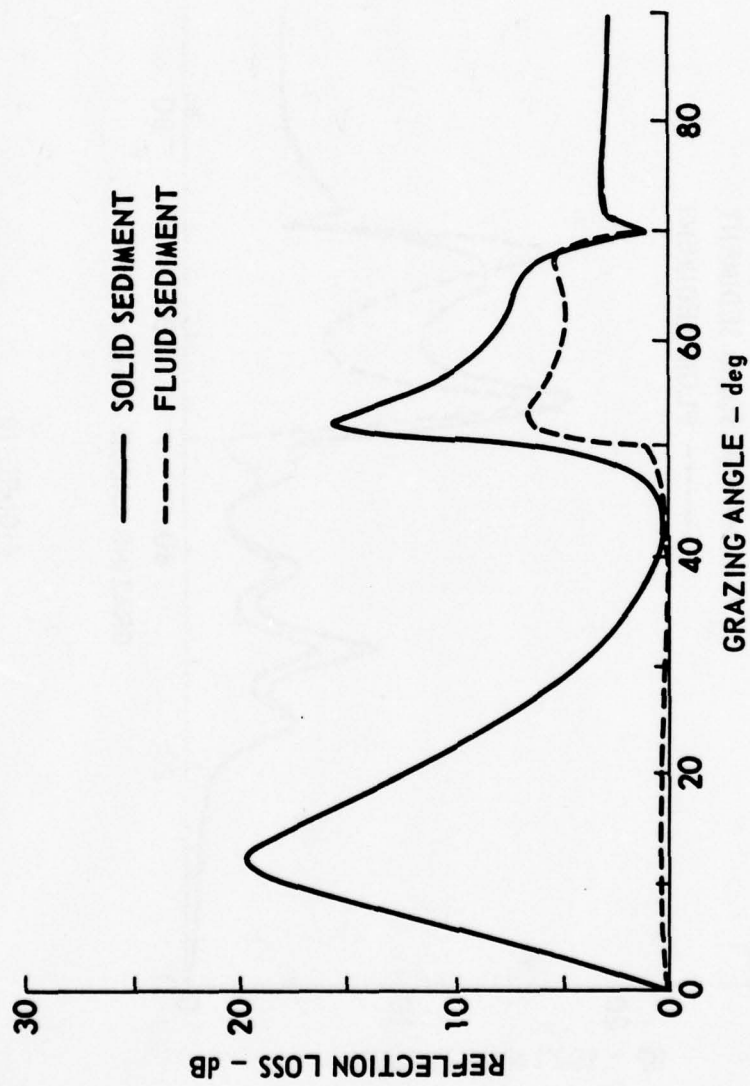


FIGURE 11
 REFLECTION LOSS versus GRAZING ANGLE FOR A 36 m
 THICK HYPOTHETICAL TURBIDITE LAYER AT 20 Hz

ARL:UT
 AS-78-1738-S
 PJV - GA
 11-27-78

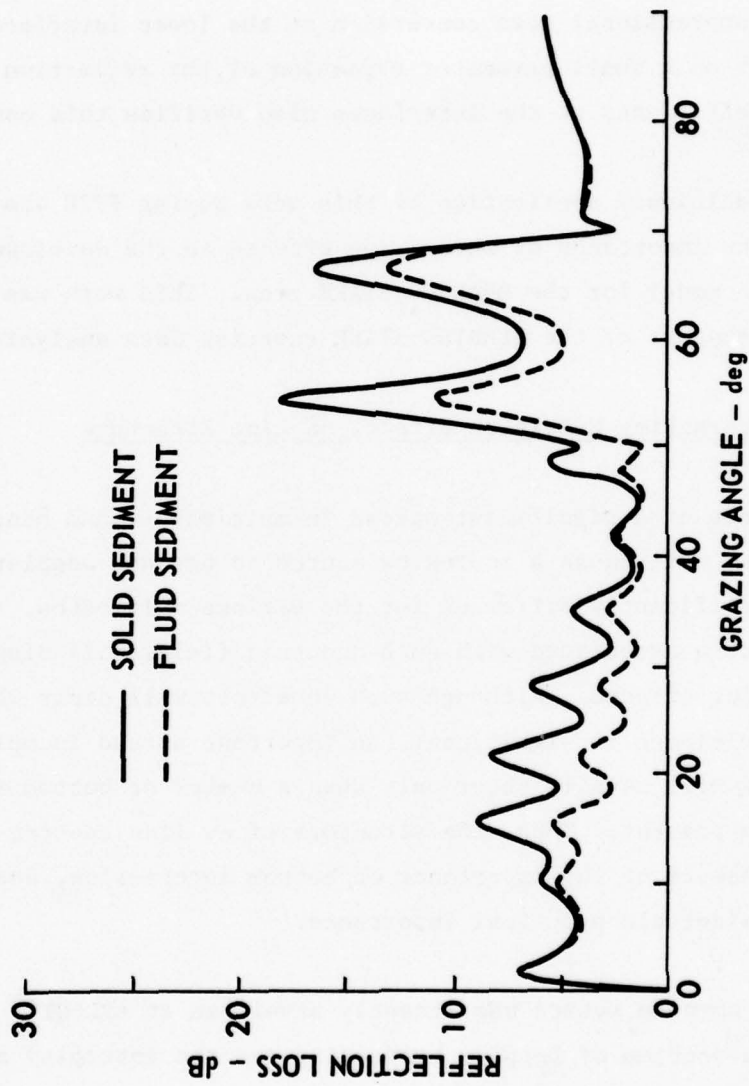


FIGURE 12
 REFLECTION LOSS versus GRAZING ANGLE FOR A 36 m
 THICK HYPOTHETICAL TURBIDITE LAYER AT 200 Hz

ARL:UT
 AS-78-1739-S
 PJV - GA
 11-27-78

increased reflection loss. If we consider the interaction of the compressional wave with the substrate, we notice that there is an angle above which the interaction is strong. For thick sediments the angle is large. As thickness decreases, the angle decreases. This is qualitatively the same dependence found for θ_0 . This similarity suggests the importance of compressional wave conversion at the lower interface. Preliminary work on a small parameter expansion of the reflection and transmission coefficients at the interfaces also verifies this conclusion.

An additional application of this work during FY78 was the estimation of the importance of shear wave effects to the development of a geoacoustic model for the BEARING STAKE area. This work was carried out in support of the BEARING STAKE exercise data analysis.

B. Bottom Interacting Multipath Effects on Line Structure

The presence of a significant spread in multipaths, and hence group velocities, will cause a moving cw source to produce Doppler effects which can be significantly different for the various multipaths. As a result, the spectra associated with such acoustic fields will display Doppler broadening effects. Although such an effect will occur whenever more than one multipath is significant, an important spread in multipath group velocities will usually occur only when a number of bottom interacting paths are present. Thus, the structure of cw line spectra provides an additional measure of the importance of bottom interaction, and one which is of considerable practical importance.

A general purpose method was recently developed at ARL:UT²⁵ to deal with the problem of Doppler broadening and the interplay of propagation effects and signal processing parameters. This method relies on a normal mode theory of the field generated by a moving source and includes a complete structured bottom as well as arbitrary source-receiver geometry. The remainder of this section will be devoted to exhibiting a number of results obtained using this model in an effort to show that the anticipated sensor geometry, source speed, and integration time dependencies are indeed obtained quantitatively.

1. Receiver and Source Depth Effects

Consider now, as an example, a source moving on a constant course at constant speed v , passing, at CPA, within 30 km of a receiver. The geometry is shown in Fig. 13 where the source-receiver range $R(t)$ will be given by $(30 \text{ km}) \times \cos \theta(t)$. Figures 14 and 15 show the results of predicted 25 Hz line spectra for a 5 m source depth and 1000 m and 4500 m receiver depths, respectively. The sound speed profile used in these calculations is taken from the CHURCH OPAL exercise area with a bottom description appropriate to this area of the North Pacific. The spectra shown here have 1 mHz resolution (1000 sec integration time). The multipath broadening effects are quite evident, as is the basic Doppler shift (upward from 25 Hz). Because the various multipaths interfere in different ways at the two receiver depths and because at the deep receiver (380 m above the bottom) there will be a higher proportion of bottom interacting energy, the details of line structure are different at these locations.

Figures 16 and 17 show the same configuration except that the source depth is 100 m rather than 5 m. Again it is observed that receiver depth affects line structure. Moreover, comparing Figs. 11 and 12, we see that the low Doppler bottom interacting modes are more important for the shallow source than for the 100 m source.

2. Range Effects

Figures 18 through 21 show a sequence of spectra for a 100 m source for ranges of 200, 100, 50, and 10 km from CPA (again, 30 km). It will be observed that as the source moves closer to the receiver the bottom interacting modes become more important, leading to more pronounced Doppler shifts for these paths. The receiver depth in these four cases is 4833 m (50 m above the bottom). It is clear from these calculations that, especially for cases of a receiver near a boundary, line shape will also depend on bottom loss.

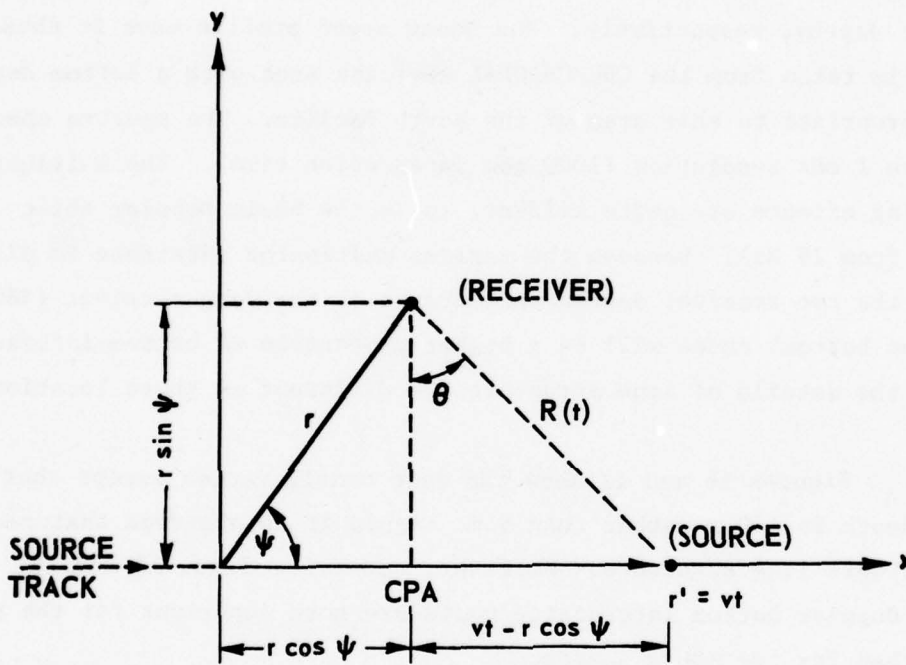


FIGURE 13
 SCHEMATIC ILLUSTRATION OF SOURCE TRACK
 AND RECEIVER GEOMETRY

ARL:UT
 AS-78-630-P
 KEH-GA
 4-19-78

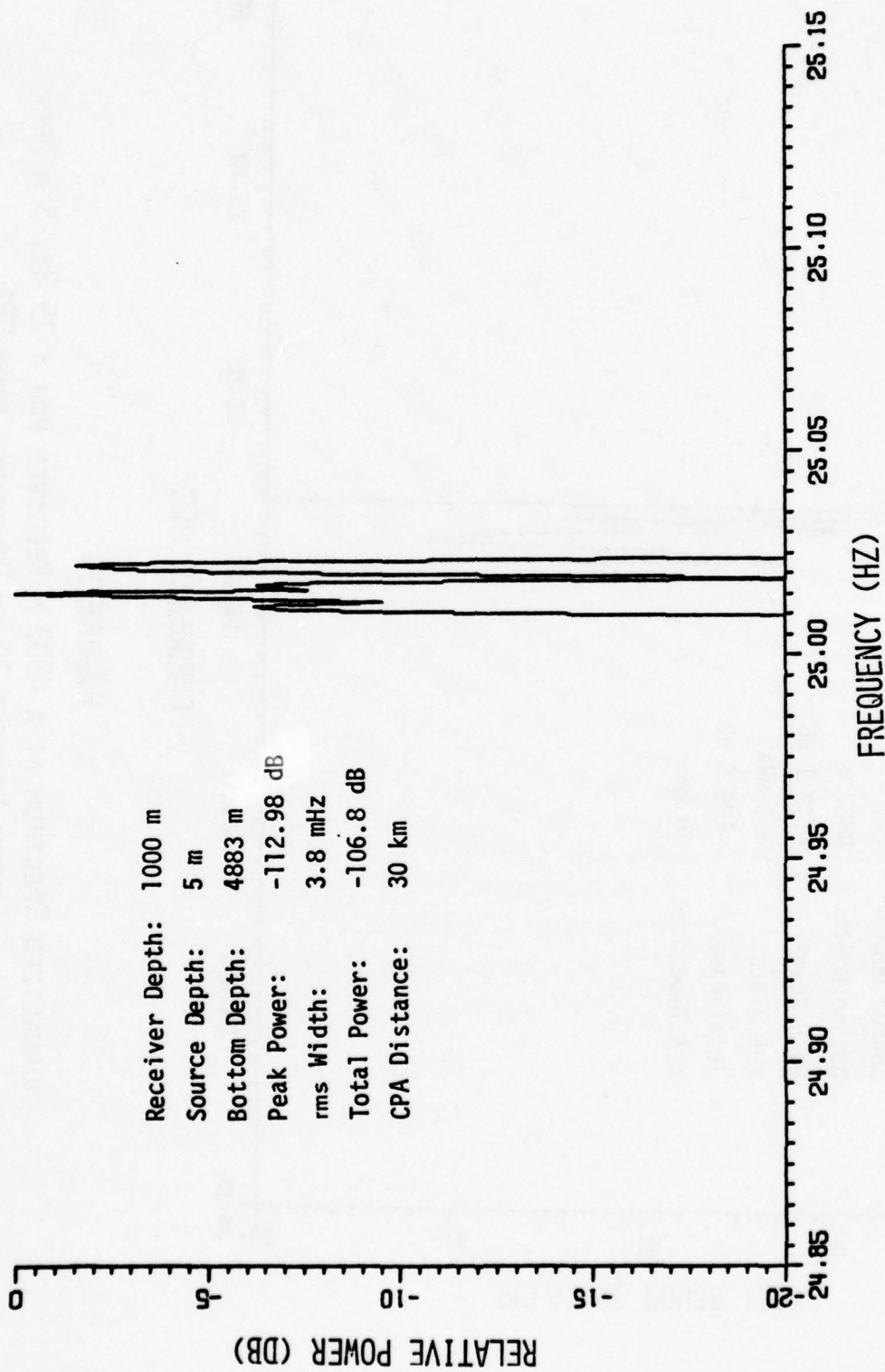
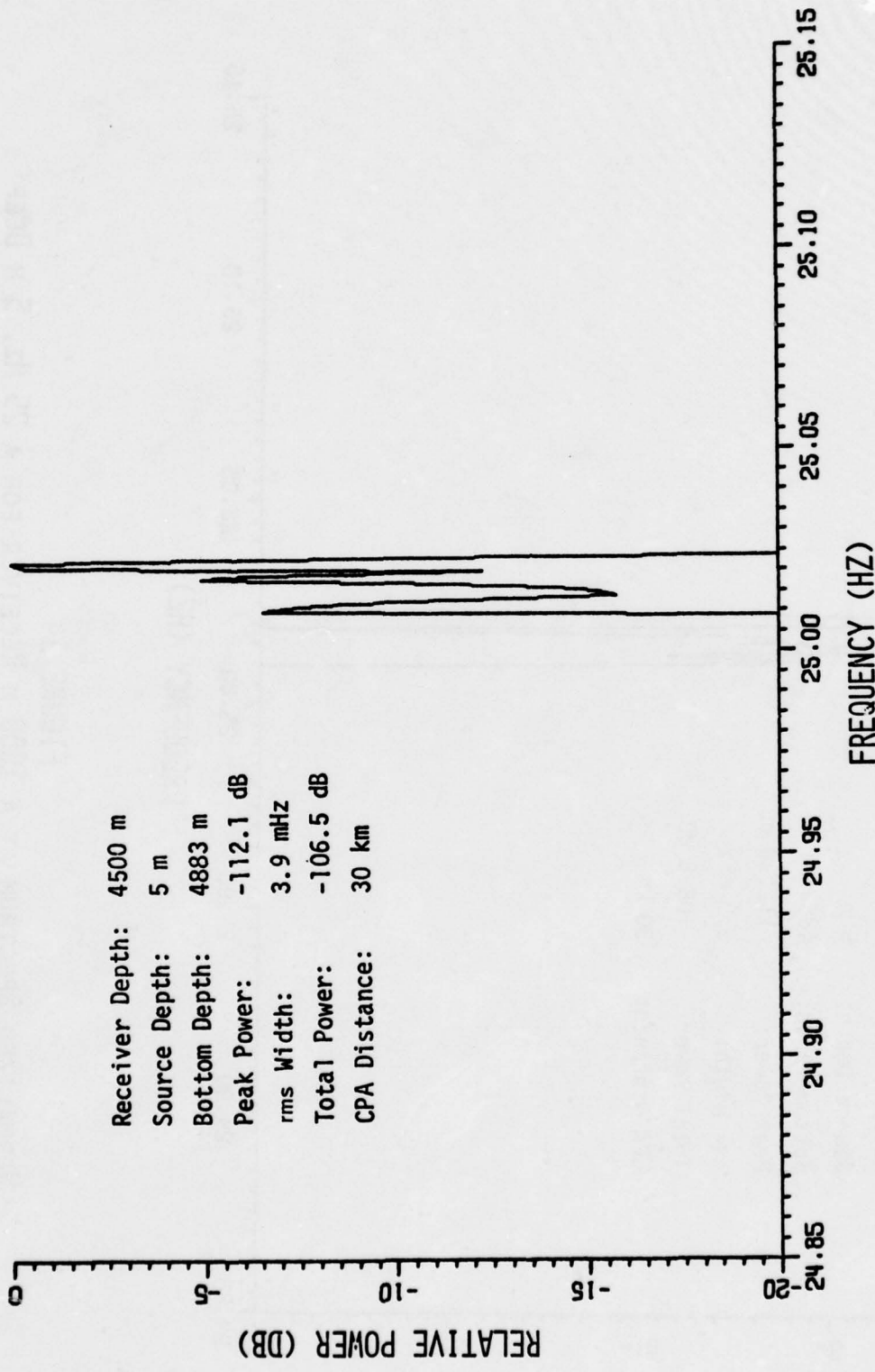


FIGURE 14
 NORMALIZED SPECTRUM AT A 1000 M RECEIVER FOR A 25 HZ, 5 M DEEP
 SOURCE LOCATED 20 KM DOWNRANGE FROM CPA



Receiver Depth: 4500 m
 Source Depth: 5 m
 Bottom Depth: 4883 m
 Peak Power: -112.1 dB
 rms Width: 3.9 mHz
 Total Power: -106.5 dB
 CPA Distance: 30 km

FIGURE 15

NORMALIZED SPECTRUM AT A 4500 M RECEIVER FOR A 25 HZ, 5 M DEEP
 SOURCE LOCATED 20 KM DOWNRANGE FROM CPA

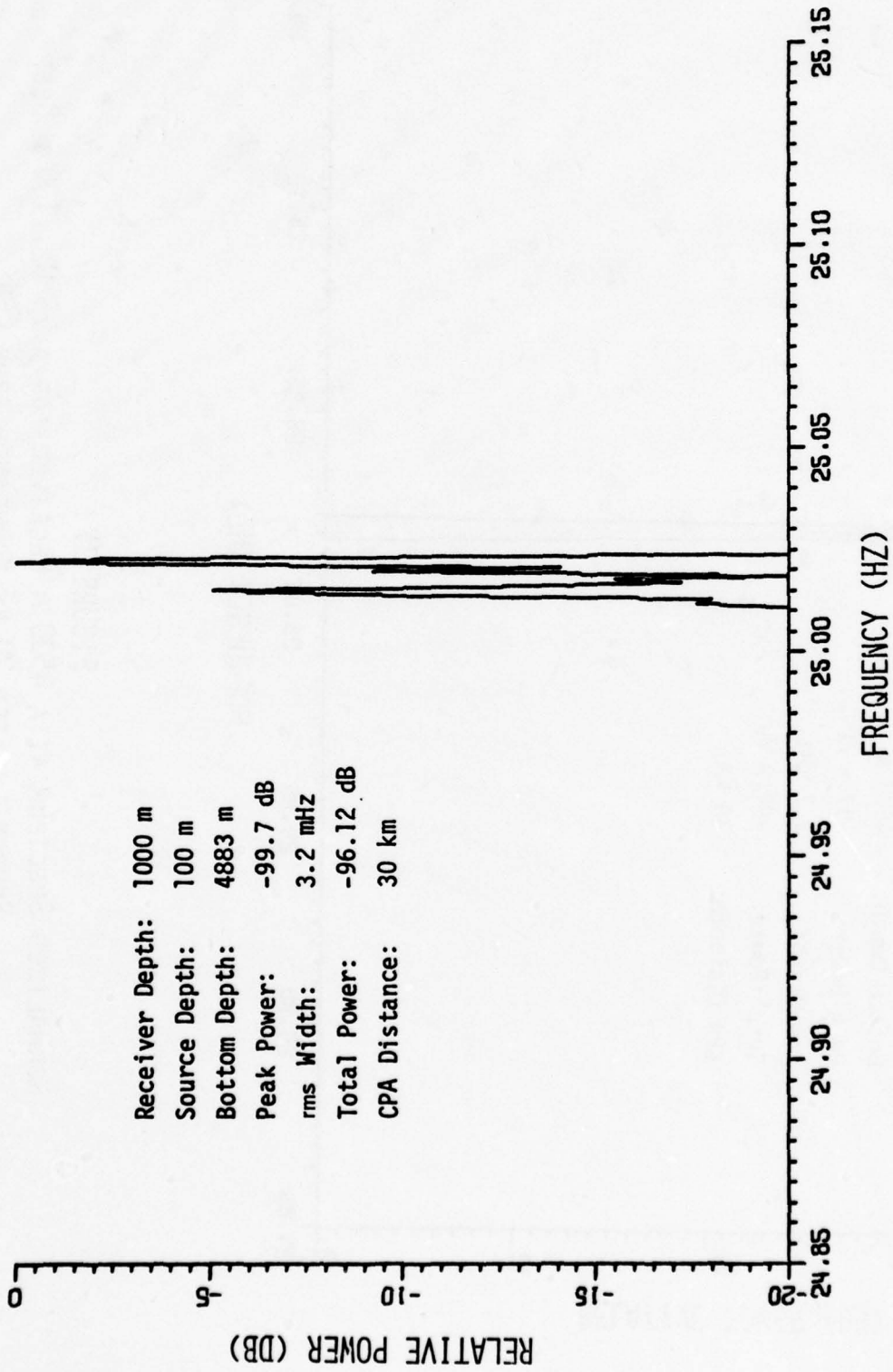


FIGURE 16
 NORMALIZED SPECTRUM AT A 1000 M RECEIVER FOR A 25 HZ, 100 M DEEP
 SOURCE LOCATED 20 KM DOWNRANGE FROM CPA

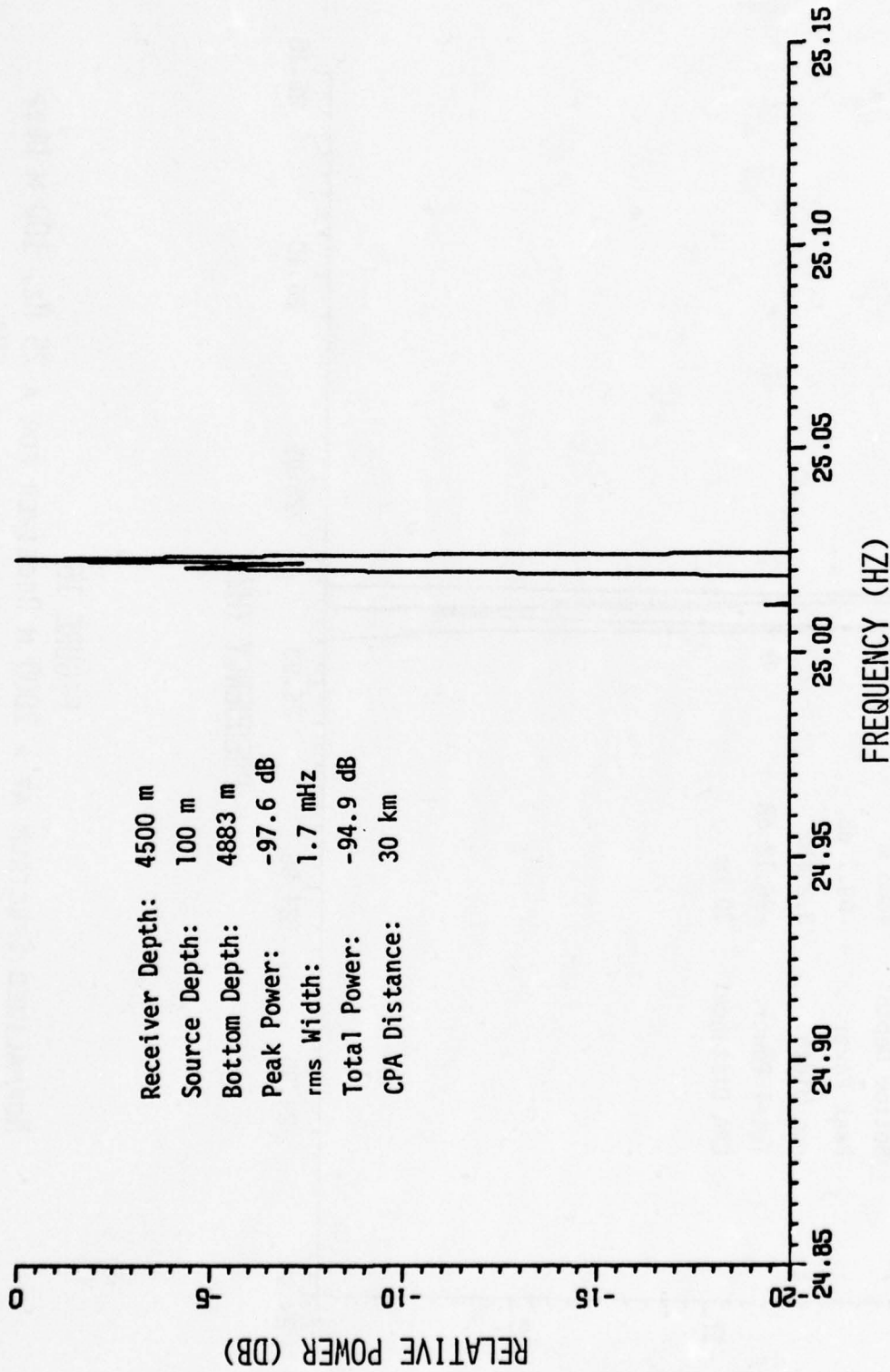


FIGURE 17

NORMALIZED SPECTRUM AT A 4500 M RECEIVER FOR A 25 HZ, 100 M DEEP
SOURCE LOCATED 20 KM DOWNRANGE FROM CPA

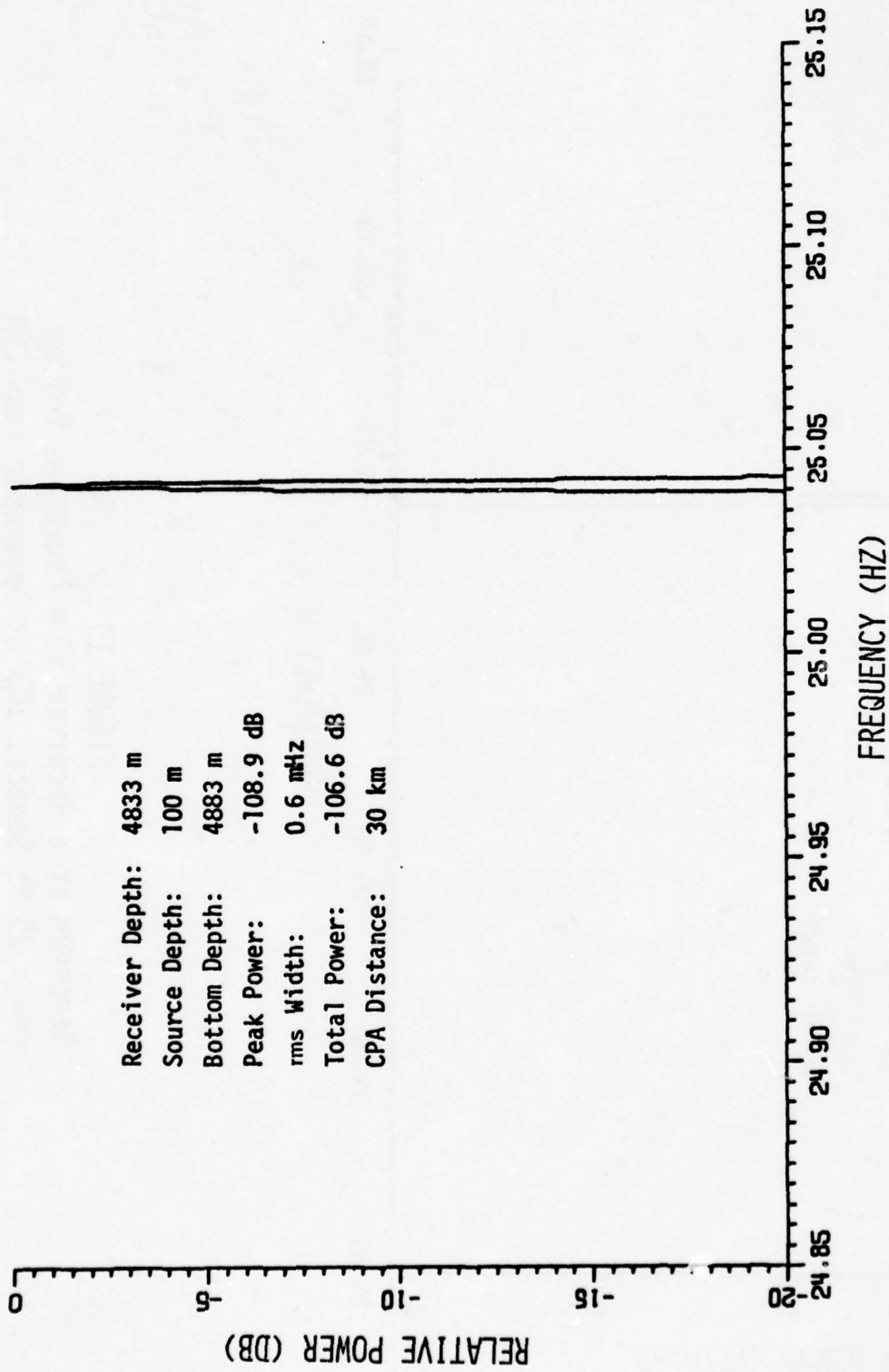
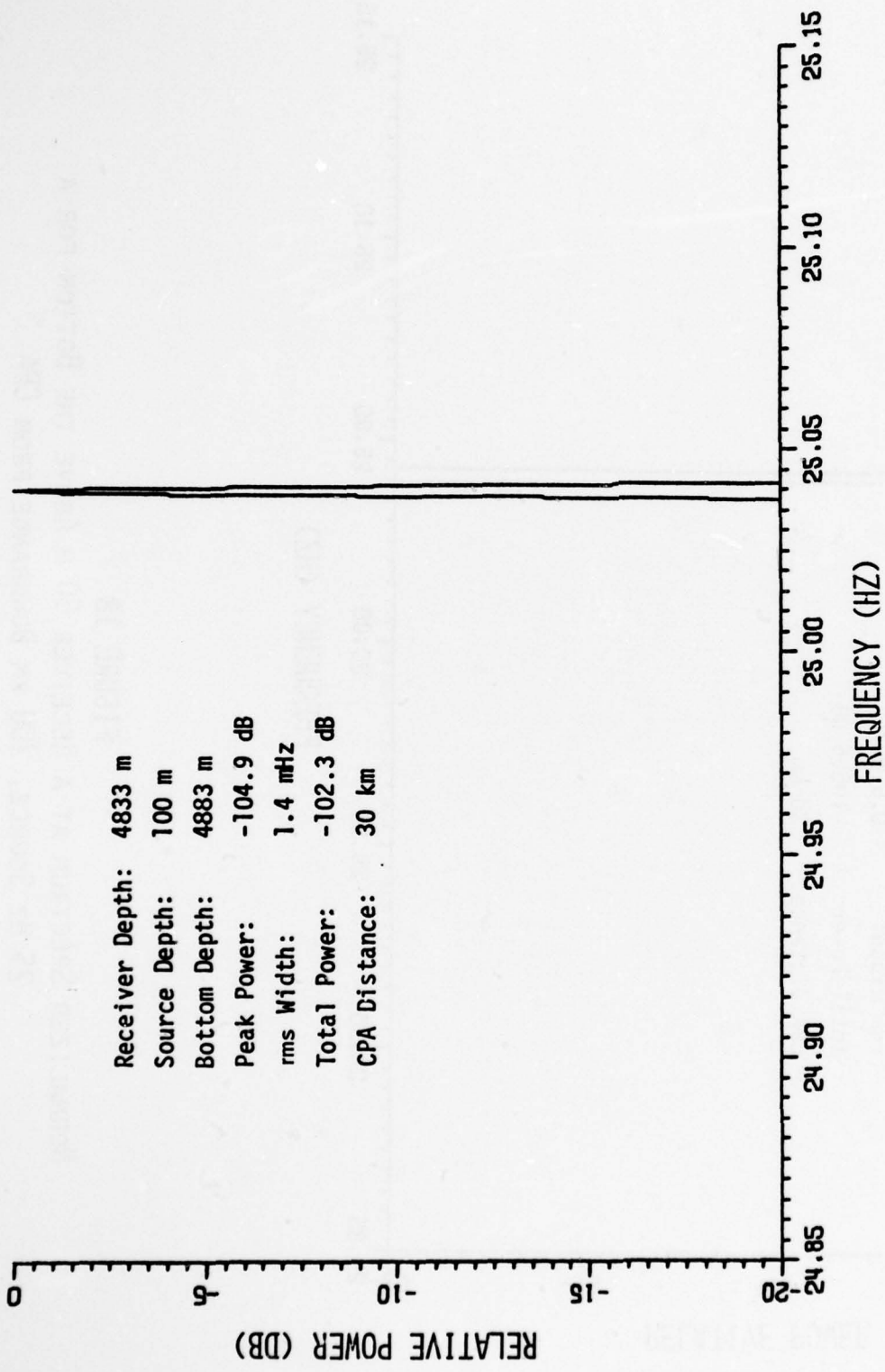


FIGURE 18
 NORMALIZED SPECTRUM AT A RECEIVER 50 M ABOVE THE BOTTOM FOR A
 25 HZ SOURCE, 200 KM DOWNRANGE FROM CPA



Receiver Depth: 4833 m
 Source Depth: 100 m
 Bottom Depth: 4883 m
 Peak Power: -104.9 dB
 rms Width: 1.4 mHz
 Total Power: -102.3 dB
 CPA Distance: 30 km

FIGURE 19
 SPECTRUM AT A RECEIVER 50 M ABOVE THE BOTTOM
 FOR A 25 HZ SOURCE, 100 KM DOWNRANGE FROM CPA

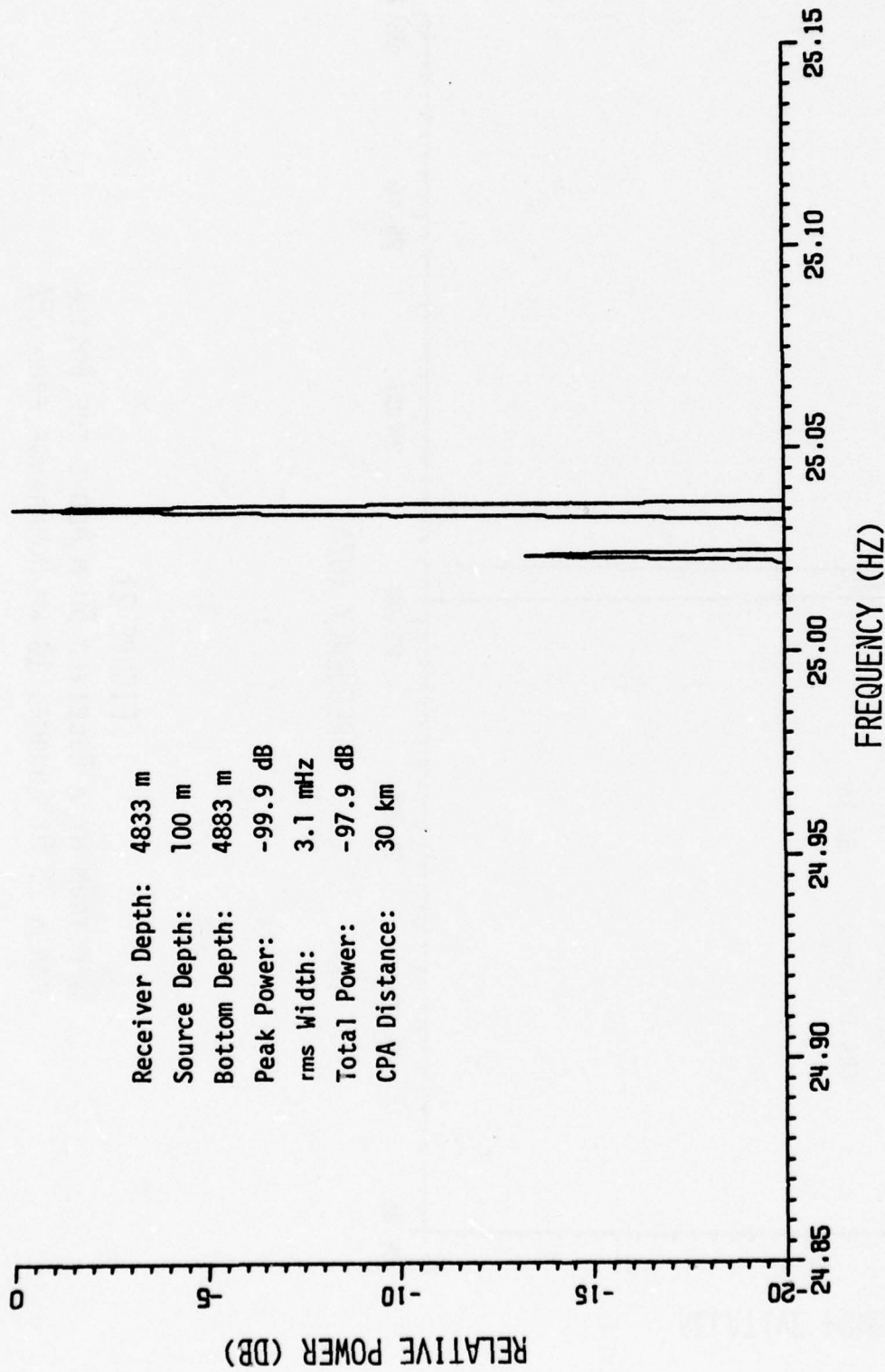


FIGURE 20
 SPECTRUM AT A RECEIVER 50 M ABOVE THE BOTTOM
 FOR A 25 HZ SOURCE, 50 KM DOWNRANGE FROM CPA

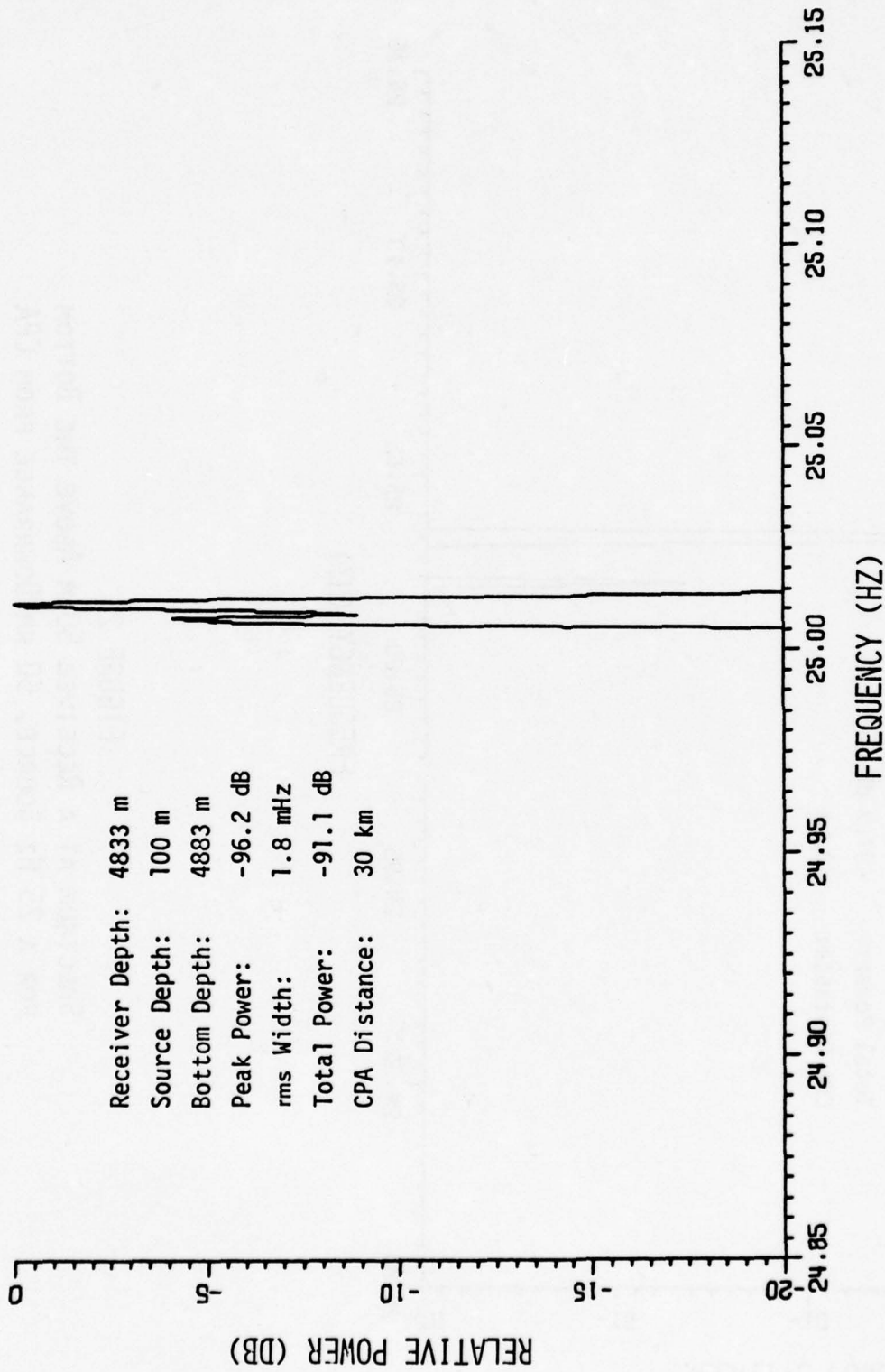


FIGURE 21
 SPECTRUM AT A RECEIVER 50 M ABOVE THE BOTTOM
 FOR A 25 HZ SOURCE, 10 KM DOWNRANGE FROM CPA

3. Source Speed Effects

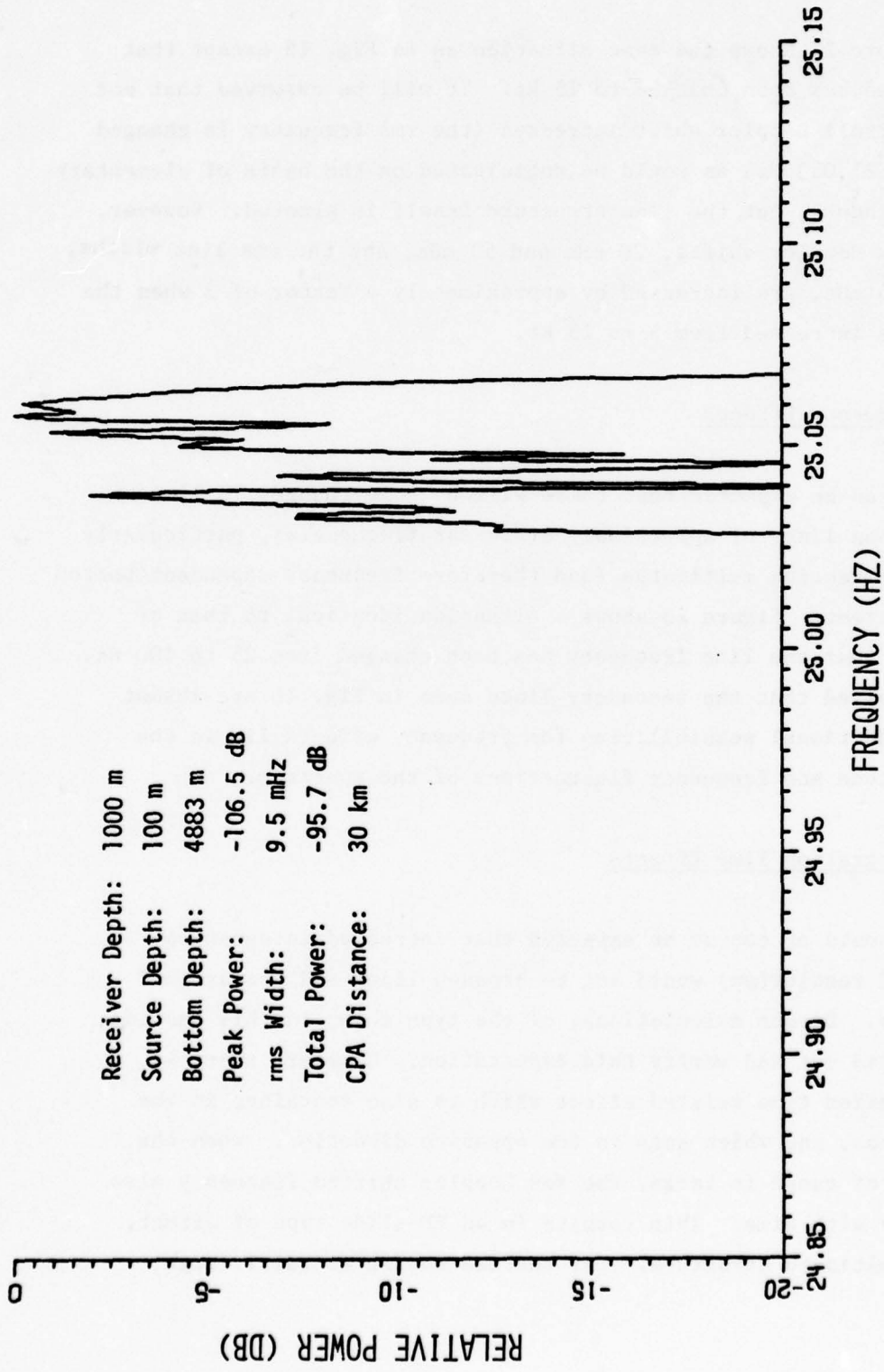
Figure 22 shows the same situation as in Fig. 15 except that the source speed has been changed to 15 kt. It will be observed that not only is the overall Doppler shift increased (the rms frequency is changed from 25.020 to 25.053 Hz) as would be anticipated on the basis of elementary Doppler shift theory, but the line structure itself is altered. However, both of the rms Doppler shifts, 20 mHz and 53 mHz, and the rms line widths, 3.2 mHz and 9.6 mHz, are increased by approximately a factor of 3 when the source speed is increased from 5 to 15 kt.

4. Frequency Effects

It can be expected that there will be some changes in line structure between lines of appreciably different frequencies, particularly when bottom interacting multipaths (and therefore frequency dependent bottom loss) are important. Figure 23 shows a situation identical to that of Fig. 16 except that the line frequency has been changed from 25 to 100 Hz. It will be observed that the secondary lines seen in Fig. 16 are absent in Fig. 23. Additional possibilities for frequency effects lie in the areas of amplitude and frequency fluctuations of the spectrum.

5. Integration Time Effects

It would of course be expected that decreased integration time (decreased resolution) would act to broaden lines and "smear out" secondary lines. Direct calculations, of the type shown in this section, have been carried out and verify this expectation. However, there is another integration time related effect which is also contained in the model predictions, and which acts in the opposite direction. When the rate of change of range is large, the rms Doppler shifted frequency also changes rapidly with time. This results in an FM-slide type of effect, whatever the multipath structure. For sources moving at fairly high



Receiver Depth: 1000 m
 Source Depth: 100 m
 Bottom Depth: 4883 m
 Peak Power: -106.5 dB
 rms Width: 9.5 mHz
 Total Power: -95.7 dB
 CPA Distance: 30 km

FIGURE 22
 NORMALIZED SPECTRUM FOR A 15 KT SOURCE
 20 KM FROM CPA, AT A 1000 M RECEIVER

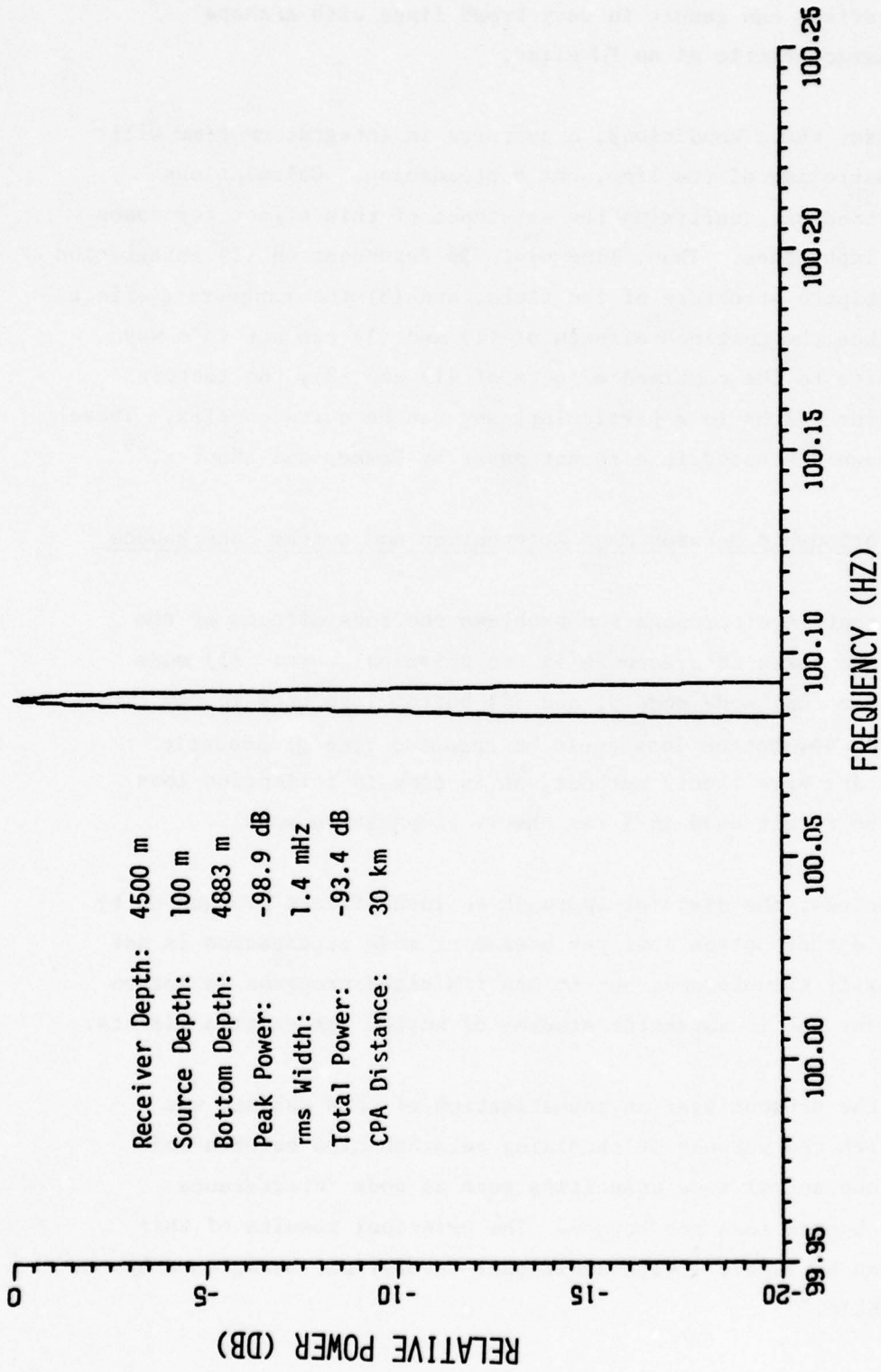


FIGURE 23
 NORMALIZED SPECTRUM FOR A 100 HZ SOURCE
 20 KM FROM CPA, AT A 4500 M RECEIVER

speeds, this effect can result in very broad lines with a shape completely characteristic of an FM slide.

Under these conditions, a decrease in integration time will result in a narrowing of the line, not a broadening. Calculations have been carried out confirming the existence of this effect for cases of practical importance. Thus, line width is dependent on (1) integration time, (2) multipath structure of the field, and (3) the range-rate effect near CPA. Since the combined effects of (1) and (3) can act in a way that is opposite to the combined effects of (1) and (2), the factors determining line widths in a particular case can be quite complex. These issues have been discussed in a recent paper by Hawker and Shooter.²⁶

C. The Relationship Between Mode Attenuation and Bottom Loss/Bounce

In the context of propagation problems the loss effects of the ocean bottom are taken into account in two principal ways: (1) mode attenuation in normal mode models, and (2) bottom loss used in ray models. Of course, bottom loss could be computed from geoacoustic description using wave theory methods, as is done in reflection loss models, and the result used in a ray theory propagation model.

Nevertheless, the disjoint approach to loss effects brought on by a reliance on either bottom loss per bounce or mode attenuation is not only conceptually troublesome, but it has inhibited progress in bottom loss measurement and in parameter studies of bottom interaction effects.

During the present year an investigation of this subject was carried out with the purpose of obtaining relationships between mode attenuation (and normal mode quantities such as mode interference distance) and bottom loss per bounce. The principal results of this study are given by Tindle²⁷ with additional theoretical background by Weston and Tindle.²⁸

The primary results of this study are twofold:

- The mode attenuation δ_n per mode interference distance $D_n = 2\pi (dn/dk_n)$ given by δ_n/D_n is essentially identical with reflection loss. This equivalence has been shown within the context of WKB theory as well as generally, using numerical computations.
- The mode interference distance was also found to be given by

$$D_n = \frac{4\gamma_1 k_n}{(\gamma_1 U_n(H))^2 + (U'_n(H))^2},$$

where U_n and U'_n are the values of the normal mode evaluated at the bottom of the water column, and $\gamma_1^2 = k_1^2 - k_n^2$.

These results are important for several reasons going beyond the conceptual advances they produce. The combination of these two results, together with the identification of $U'_n(H)/U_n(H)$ with a particular function of the reflection coefficient, opens the possibility of normal mode computation based on bottom loss rather than a geoacoustic subbottom description. Although a major thrust of this overall bottom interaction research program has been to emphasize the utility of a geoacoustic description, the existence of a large body of measured bottom loss data requires that bottom loss be a possible input in propagation models.

V. SUPPORT ACTIVITIES

With the analytic intractability of many of the acoustic equations, computer assisted numerical computation serves a vital function in the bottom interaction program. The acquisition of the CYBER 171 by ARL:UT in January 1978 has greatly improved the computing capabilities of this laboratory. Tasks formerly regarded as infeasible due to limited core and disk space and excessive computation time can now be performed.

During 1978, the major software tools previously developed by the bottom interaction program, including the ray and mode models and the bottom loss reflection model, were converted to CYBER compatible FORTRAN. Some of these models were restructured and/or expanded to enable more efficient use of the computer.

The major software development during this year was an extension of the existing BOTLOSS (bottom loss reflection) model. Previously dealing only with fluid sediments, this model will now compute effects due to shear waves in the sediments. The program has been extensively tested and is being used in production runs. The software package centered around the normal mode model was enlarged by the design and implementation of a model calculating the time series and line structure generated by a moving source.

A laboratory-wide computer terminal network was set up in April, and with this means of easy access to the CYBER, usage of all software was greatly increased. It became apparent that most users were unable to take advantage of the sophisticated models due to their incomplete knowledge of programming, job operations, and/or specific model requirements. To remedy this and to provide easy and effective use of all production models, a model operating system was initiated. This system facilitates the running of the models, reduces the possibility of errors, and requires only a very limited knowledge of CYBER job control. All

bottom interaction software has been incorporated into this system, and consequently has been used extensively. Computer accessible documentation directing the use of this system has been installed. A library of sound speed profiles is also available via terminal interaction.

ACKNOWLEDGMENTS

The authors wish to acknowledge the very important role played in this research program by Terry Foreman, Ruth Gonzalez, and Susan Payne, who are responsible for all of the computer software necessary for the studies described here. In several cases these software developments have entailed substantial advances in the state-of-the-art in computational acoustics.

Also, the authors wish to acknowledge the substantial benefits of numerous discussions with Chris Tindle, The University of Auckland, New Zealand, and C. W. Horton, Sr., ARL:UT.

REFERENCES

1. A. D. Pierce, "Extension of the method of normal modes to sound propagation in an almost-stratified medium," J. Acoust. Soc. Am. 37, 19-27 (1965).
2. D. M. Milder, "Ray and wave invariants for SOFAR channel propagation," J. Acoust. Soc. Am. 46, 1259-1263 (1969).
3. S. R. Rutherford and K. E. Hawker, "An examination of the influence of the range dependence of the ocean bottom on the adiabatic approximation," submitted to The Journal of The Acoustical Society of America.
4. S. R. Rutherford and K. E. Hawker, "An Examination of the Coupling Coefficients of a Coupled Mode Theory," presented at the Fall Meeting, The American Geophysical Union, San Francisco, California, Paper O214, December 1978.
5. C. T. Tindle and K. M. Guthrie, "Rays as interfering modes in underwater acoustics," J. Sound Vib. 34, 291-295 (1974).
6. W. A. Kuperman, "Coherent component of specular reflection and transmission at a randomly rough two-fluid interface," J. Acoust. Soc. Am. 61, 365-370 (1975).
7. W. A. Kuperman and F. Ingenito, "Attenuation of the coherent component of sound propagating in shallow water with rough boundaries," J. Acoust. Soc. Am. 61, 1178-1187 (1977).
8. S. R. Rutherford, K. E. Hawker, and S. G. Payne, "A study of the effects of ocean bottom roughness on low frequency sound propagation," J. Acoust. Soc. Am. 65, 381-386 (1979).
9. K. E. Hawker and T. L. Foreman, "A plane wave reflection loss model based on numerical integration," J. Acoust. Soc. Am. 64, 1470-1477 (1978).
10. S. R. Rutherford and K. E. Hawker, "The effects of density gradients on bottom reflection loss for a class of marine sediments," J. Acoust. Soc. Am. 63, 750-757 (1978).
11. K. E. Hawker, W. E. Williams, and T. L. Foreman, "A study of the acoustical effects of subbottom absorption profiles," J. Acoust. Soc. Am. 65, 360-367 (1979).

12. K. E. Hawker, "The influence of Stoneley waves on plane wave reflection coefficients: characteristics of bottom reflection loss," J. Acoust. Soc. Am. 64, 548-555 (1978).
13. K. E. Hawker, "Existence of Stoneley waves as a loss mechanism in plane wave reflection problems," J. Acoust. Soc. Am. 65, 682-686 (1979).
14. E. L. Hamilton, "Shear-wave velocity versus depth in marine sediments: a review," Geophysics 41, 985-996 (1976).
15. E. L. Hamilton, "Attenuation of shear waves in marine sediments," J. Acoust. Soc. Am. 60, 334-338 (1976).
16. D. J. Shirley and L. D. Hampton, "Shear wave measurements in laboratory sediments," J. Acoust. Soc. Am. 63, 607-613 (1978).
17. P. G. Richards, "Weakly coupled potentials for high-frequency elastic waves in continuously stratified media," Bull. Seism. Soc. Am. 64, 1575-1588 (1974).
18. W. T. Thomson, "Transmission of elastic waves through a stratified solid medium," J. Appl. Phys. 21, 89-93 (1950).
19. N. A. Haskell, "The dispersion of surface waves on multilayered media," Bull. Seism. Soc. Am. 43, 17-34 (1953).
20. F. Gilbert and G. E. Backus, "Propagator matrices in elastic wave and vibration problems," Geophysics 31, 326-332 (1966).
21. E. L. Hamilton, "Sound attenuation as a function of depth in the sea floor," J. Acoust. Soc. Am. 59, 528-535 (1976).
22. E. L. Hamilton, "Attenuation of shear waves in marine sediments," J. Acoust. Soc. Am. 60, 334-338 (1976).
23. G. J. Fryer, "Reflectivity of the ocean bottom at low frequency," J. Acoust. Soc. Am. 63, 35-42 (1978).
24. P. J. Vidmar and T. L. Foreman, "The effect of sediment rigidity on the acoustic reflectivity of the ocean bottom," EOS, Trans. Am. Geophys. Union 59, 1119 (1978).
25. K. E. Hawker, "A normal mode theory of acoustic Doppler effects in the oceanic waveguide," J. Acoust. Soc. Am. 65, 675-686 (1979).
26. K. E. Hawker and J. A. Shooter, "The Roles of Integration Time and Acoustic Multipaths in Determining the Structure of cw Line Spectra," Proceedings of the IEEE ICASSP Conference, April 1979.

27. C. T. Tindle, "The equivalence of bottom loss and mode attenuation per cycle in underwater acoustics," to be published in The Journal of The Acoustical Society of America.
28. D. E. Weston and C. T. Tindle, "Reflection loss and mode attenuation in a Pekeris model," submitted for publication in The Journal of The Acoustical Society of America.

5 March 1979

DISTRIBUTION LIST FOR
 ARL-TR-79-2
 ANNUAL REPORT UNDER CONTRACT N00014-78-C-0113
 UNCLASSIFIED

Copy No.

- Commanding Officer
 Naval Ocean Research and Development Activity
 NSTL Station, MS 39529
- 1 Attn: CDR J. Paquin (Code 500)
 2 R. D. Gaul (Code 600)
 3 CDR T. McCloskey (Code 200)
 4 S. W. Marshall (Code 340)
 5 H. Eppert (Code 360)
 6 A. L. Anderson (Code 320)
 7 M. G. Lewis (Code 500)
 8 J. Matthews (Code 360)
 9 G. Morris (Code 340)
 10 R. R. Goodman
- Commanding Officer
 Office of Naval Research
 Arlington, VA 22217
- 11 Attn: J. B. Hersey (Code 102-OS)
 12 A. Sykes
 13 T. Pyle (Code 430)
 14 H. Bezdek (Code 460)
 15 M. McKisic (Code 486)
- 16 Office of Naval Research
 Department of the Navy
 Chicago Branch Office
 536 South Clark Street
 Chicago, IL 60605
- Commanding Officer
 Naval Electronic Systems Command
 Washington, DC 20360
- 17 Attn: J. Sinsky (Code 320)
 18 J. Cybulski (Code 320)
 19 CDR D. Griffiths (Code 320)
 20 Code PME 124-30
 21 Code PME 124-62
 22 E. Tunstall (Code 124TA)

Distribution List for ARL-TR-79-2, Annual Report under Contract
N00014-78-C-0113, (Cont'd).

Copy No.

Director
Naval Research Laboratory
Department of the Navy
Washington, DC 20375
23 Attn: R. H. Ferris
24 B. B. Adams (Code 8160)
25 Code 2627
26 O. Diachok
27 A. Gerlach
28 B. G. Hurdle

Commanding Officer
Naval Ocean Systems Center
Department of the Navy
San Diego, CA 92152
29 - 30 Attn: E. L. Hamilton
31 R. R. Gardner
32 M. A. Pederson
33 H. P. Bucker
34 D. Gordon
35 O. D. Grace

Commander
Naval Sea Systems Command
Department of the Navy
Washington, DC 20362
36 Attn: C. D. Smith (Code 06H1)
37 A. P. Franceschetti

Chief of Naval Operations
Department of the Navy
Washington, DC 20350
38 Attn: R. S. Winokur (OP95E1)

Chief of Naval Material
Department of the Navy
Washington, DC 20360
39 Attn: G. R. Spalding (Code 08T24)
40 CDR E. Young (Code 08T24)

Commander
Naval Intelligence Support Center
Department of the Navy
4301 Suitland Road
Washington, DC 20390
41 Attn: Code 222

Distribution List for ARL-TR-79-2, Annual Report under Contract
N00014-78-C-0113, (Cont'd)

Copy No.

42 Commander
 Naval Surface Weapons Center
 White Oak Laboratory
 Department of the Navy
 Silver Spring, MD 20910

43 Commander
 David W. Taylor Naval Ship Research and
 Development Center
 Department of the Navy
 Bethesda, MD 20034

 Naval Oceanographic Office
 Department of the Navy
 Washington, DC 20373

44 - 45 Attn: W. H. Geddes

 Commander
 Naval Air Development Center
 Department of the Navy
 Warminster, PA 18974

46 Attn: P. Van Schuyler (Code 2052)

47 C. L. Bartberger

48 P. Haas

 Officer in Charge
 New London Laboratory
 Naval Underwater Systems Center
 Department of the Navy
 New London, CT 06320

49 Attn: F. R. DiNapoli

50 R. Deavenport

51 J. Papadakis

52 R. Lauer

53 P. Herstein

54 R. Hasse

55 Assistant Director
 Ocean Control DDR & E
 Room 3D, 1048 Pentagon
 Washington, DC 20301

 OASN (R, E & S)
 Room 4D, 745 Pentagon
 Washington, DC 20301

56 Attn: G. A. Cann

Distribution List for ARL-TR-79-2, Annual Report under Contract
NO0014-78-C-0113, (Cont'd)

Copy No.

57 Defense Advanced Research Projects Agency
Acoustic Research Center
Moffett Field, CA 94035
Attn: E. Smith

58 Superintendent
Naval Postgraduate School
Monterey, CA 93940
Attn: Library

59 H. Medwin

60 O. B. Wilson

61 Commanding Officer
Naval Air Systems Command
Department of the Navy
Washington, DC 20361
Attn: CDR J. Messegee (Code PMA-264)

62 - 63 Commanding Officer and Director
Defense Documentation Center
Cameron Station, Building 5
5010 Duke Street
Alexandria, VA 22314

64 Arthur D. Little, Inc.
15 Acorn Park
Cambridge, MA 02140
Attn: G. Raisbeck

65 Woods Hole Oceanographic Institution
86-96 Water Street
Woods Hole, MA 02543
Attn: E. E. Hays

66 G. Frisk

67 R. Spindel

68 Science Applications, Inc.
8400 Westpark Drive
McLean, VA 22101
Attn: J. Hanna

69 C. Spofford

70 L. Dozier

71 Applied Research Laboratory
The Pennsylvania State University
P.O. Box 30
State College, PA 16801
Attn: S. McDaniel

Distribution List for ARL-TR-79-2, Annual Report under Contract
N00014-78-C-0113, (Cont'd)

Copy No.

72	Underwater Systems, Inc. World Building 8121 Georgia Avenue Silver Spring, MD 20910 Attn: M. S. Weinstein
73	Marine Physical Laboratory of The Scripps Institution of Oceanography The University of California, San Diego San Diego, CA 92132 Attn: V. Anderson
74	F. Fisher
75	G. Shor
76	Tracor, Inc. 1601 Research Boulevard Rockville, MD 20850 Attn: J. Gottwald
77	A. Wittenborn
78	R. J. Urick
79	Bell Telephone Laboratories, Inc. Whippany Road Whippany, NJ 07961 Attn: S. A. Kramer
80	Planning Systems, Inc. 7900 Westpark Drive, Suite 507 McLean, VA 22101 Attn: L. Solomon
81	TRW, Inc. TRW Defense & Space Systems Group Washington Operations 7600 Colshire Drive McLean, VA 22101 Attn: R. T. Brown
82	I. Gereben
83	SUTRON Corporation Suite 700 1923 North Lynn Street Arlington, VA 22209 Attn: C. Dabney

Distribution List for ARL-TR-79-2, Annual Report under Contract
N00014-78-C-0113 (Cont'd)

Copy No.

84 Daubin Systems Corporation
104 Crandon Boulevard
Key Biscayne, FL 33149
Attn: S. Daubin

85 Defence Scientific Establishment
HMNZ Dockyard
Devonport, Auckland
NEW ZEALAND
Attn: K. M. Guthrie

86 R. N. Denham

87 R. Bannister

88 Physics Department
The University of Auckland
Private Bag, Auckland
NEW ZEALAND
Attn: A. C. Kibblewhite

89 G. Bold

90 C. T. Tindle

91 The Catholic University of America
Washington, DC 20064
Attn: H. M. Uberall

92 Department of Geology and Geophysics
Geophysical and Polar Research Center
Lewis G. Weeks Hall for Geological Sciences
The University of Wisconsin, Madison
1215 W. Dayton Street
Madison, WI 53706
Attn: C. S. Clay

93 Courant Institute
251 Mercer Street
New York, NY 10012
Attn: D. C. Stickler

94 Commander
Naval Coastal Systems Center
Department of the Navy
Panama City, FL 32407
Attn: G. McLeroy

Distribution List for ARL-TR-79-2, Annual Report under Contract
N00014-78-C-0113 (Cont'd)

Copy No.

95	Bolt, Beranek, and Newman, Inc. 50 Moulton Street Cambridge, MA 02138 Attn: P. W. Smith, Jr.
96	Boeing Aerospace Corporation Advanced Projects P.O. Box 3999, M.S. 84-63 Seattle, WA 98124 Attn: Bob Arnold
97	The Institute of Acoustic Research 615 SW 2nd Avenue Miami, FL 33130 Attn: M. Kronengold
98	J. Clark
99	Massachusetts Institute of Technology Department of Ocean Engineering Cambridge, MA 02139 Attn: Professor I. Dyer
100	The Lamont-Doherty Geological Observatory Columbia University Palisades, NY 10964 Attn: R. D. Stoll
101	H. A. Kutschale
102	Hawaii Institute of Geophysics The University of Hawaii 2525 Corres Road Honolulu, HI 96822 Attn: G. Sutton
103	G. Fryer
104	Director North Atlantic Treaty Organization SACLANT ASW Research Centre APO, NY 09019 Attn: T. Akal
105	F. Jensen
106	D. Ross
107	W. Kuperman

Distribution List for ARL-TR-79-2, Annual Report under Contract
N00014-78-C-0113 (Cont'd)

Copy No.

108	Defence Research Establishment Pacific CF Dockyard Victoria, B.C., CANADA Attn: G. R. Ebbeson
109	Defence Research Establishment Atlantic 9 Grove Street P.O. Box 1012 Dartmouth, N.S., CANADA Attn: I. Fraser
110	D. Chapman
111	Rosensteil School of Marine and Atmospheric Science The University of Miami 10 Rickenbacker Causeway Miami, FL 33149 Attn: Dr. H. DeFerrari
112	Applied Physics Laboratory The Johns Hopkins University Johns Hopkins Road Laurel, MD 20810 Attn: L. H. Wallman
113	Bell Telephone Laboratories Whippany Road Whippany, NJ 07961 Attn: F. Labianca
114	Polar Research Laboratory, Inc. 123 Santa Barbara Street Santa Barbara, CA 93101 Attn: B. M. Buck
115	The University of Miami 10 Rickenbacker Causeway Miami, FL 33149 Attn: Dr. F. Tappert
116	Geophysics Laboratory Marine Science Institute The University of Texas 700 The Strand Galveston, TX 77550 Attn: J. Worzel

Distribution List for ARL-TR-79-2, Annual Report under Contract
N00014-78-C-0113 (Cont'd)

Copy No.

117	Department of Geology The University of Texas at Austin Austin, TX 78712 Attn: Dr. M. M. Backus
118	Department of Electrical Engineering The University of Texas at Austin Austin, TX 78712 Attn: Dr. E. Hixon
119	School of Mechanical Engineering Georgia Institute of Technology Atlanta, GA 30332 Attn: Dr. A. D. Pierce
120	Department of Geology The University of Texas at Austin Austin, TX 78712 Attn: Dr. Clark Wilson
121	Defense Advanced Research Projects Agency 1400 Wilson Boulevard Arlington, VA 22209 Attn: T. Kooij
122	Office of Naval Research Resident Representative Room No. 582, Federal Bldg. Austin, TX 78701
123	Glen E. Ellis, ARL:UT
124	Terry L. Foreman, ARL:UT
125	Ruth Gonzalez, ARL:UT
126	Loyd D. Hampton, ARL:UT
127	Kenneth E. Hawker, ARL:UT
128	John J. Lemmon, ARL:UT
129	Stephen K. Mitchell, ARL:UT
130	Susan G. Payne, ARL:UT
131	Steven R. Rutherford, ARL:UT

Distribution List for ARL-TR-79-2, Annual Report under Contract
N00014-78-C-0113 (Cont'd)

Copy No.

132	Jack A. Shooter, ARL:UT
133	Clark S. Penrod, ARL:UT
134	Dana S. Hougland, ARL:UT
135	Paul J. Vidmar, ARL:UT
136	Reuben H. Wallace, ARL:UT
137	Karen E. Cumella, ARL:UT
138	Claude W. Horton, Sr., ARL:UT
139	A. O. Williams, Jr., ARL:UT
140	Garland R. Barnard, ARL:UT
141	Library, ARL:UT
142-171	Reserve, ARL:UT